JPL PUBLICATION 77-3

A Lightweight Solar Array Study

National Aeronautics and
Space Administration

Jet Propulsion Laboratory
California Institute of Technology
Pasadena, California 91103

1. Report No. 77-3	2. Government Accession No.	3. Recipient's Catalog No.
4. Title and Subtitle A LIGHTWEIGHT SOLAR ARRAY STUDY		5. Report Date February 15, 1977
		6. Performing Organization Code
7. Author(s) Robert H. Josephs		8. Performing Organization Report No.
9. Performing Organization Name and Address JET PROPULSION LABORATORY California Institute of Technology 4800 Oak Grove Drive Pasadena, California 91103		10. Work Unit No.
		11. Contract or Grant No. NAS 7-100
		13. Type of Report and Period Covered JPL Publication
12. Sponsoring Agency Name and Address NATIONAL AERONAUTICS AND SPACE ADMINISTRATION Washington, D.C. 20546		
		14. Sponsoring Agency Code

15. Supplementary Notes

16. Abstract

A sample module was assembled to model a portion of a flexible extendable solar array, a type that promises to become the next generation of solar array design. The resulting study of this module is intended to provide technical support to the array designer for lightweight component selection, specifications, and tests.

Selected from available lightweight components were 127-micron-thick wrap-around contacted solar cells, 34-micron-thick sputtered glass covers, and as a substrate a 13-micron-thick polyimide film clad with a copper printed circuit. Each component displayed weaknesses. The thin solar cells had excessive breakage losses. Sputtered glass cover adhesion was poor, and the covered cell was weaker than the cell uncovered. Thermal stresses caused some cell delamination from the model solar array substrate.

17. Key Words (Selected by Author(s)) Spacecraft Design, Testing and Performance Spacecraft Propulsion and Power Composite Materials Space Sciences (General)	18. Distribution Statement Unclassified -- Unlimited		
19. Security Classif. (of this report) Unclassified	20. Security Classif. (of this page) Unclassified	21. No. of Pages 31	22. Price

HOW TO FILL OUT THE TECHNICAL REPORT STANDARD TITLE PAGE

Make items 1, 4, 5, 9, 12, and 13 agree with the corresponding information on the report cover. Use all capital letters for title (item 4). Leave items 2, 6, and 14 blank. Complete the remaining items as follows:

3. Recipient's Catalog No. Reserved for use by report recipients.

7. Author(s). Include corresponding information from the report cover. In addition, list the affiliation of an author if it differs from that of the performing organization.

8. Performing Organization Report No. Insert if performing organization wishes to assign this number.

10. Work Unit No. Use the agency-wide code (for example, 923-50-10-06-72), which uniquely identifies the work unit under which the work was authorized. Non-NASA performing organizations will leave this blank.

11. Insert the number of the contract or grant under which the report was prepared.

15. Supplementary Notes. Enter information not included elsewhere but useful, such as: Prepared in cooperation with... Translation of (or by)... Presented at conference of... To be published in...

16. Abstract. Include a brief (not to exceed 200 words) factual summary of the most significant information contained in the report. If possible, the abstract of a classified report should be unclassified. If the report contains a significant bibliography or literature survey, mention it here.

17. Key Words. Insert terms or short phrases selected by the author that identify the principal subjects covered in the report, and that are sufficiently specific and precise to be used for cataloging.

18. Distribution Statement. Enter one of the authorized statements used to denote releasability to the public or a limitation on dissemination for reasons other than security of defense information. Authorized statements are "Unclassified-Unlimited, " "U. S. Government and Contractors only, " "U. S. Government Agencies only, " and "NASA and NASA Contractors only. "

19. Security Classification (of report). NOTE: Reports carrying a security classification will require additional markings giving security and downgrading information as specified by the Security Requirements Checklist and the DoD Industrial Security Manual (DoD 5220. 22-M).

20. Security Classification (of this page). NOTE: Because this page may be used in preparing announcements, bibliographies, and data banks, it should be unclassified if possible. If a classification is required, indicate separately the classification of the title and the abstract by following these items with either "(U)" for unclassified, or "(C)" or "(S)" as applicable for classified items.

21. No. of Pages. Insert the number of pages.

22. Price. Insert the price set by the Clearinghouse for Federal Scientific and Technical Information or the Government Printing Office, if known.

Preface

The work in this report was performed by the Control and Energy Conversion Division of the Jet Propulsion Laboratory.

Acknowledgment

Contents

Tables

Figures

Abstract

A sample module was assembled to model a portion of a flexible extendable solar array, a type that promises to become the next generation of solar array design. The resulting study of this module is intended to provide technical support to the array designer for lightweight component selection, specifications, and tests.

Selected from available lightweight components were 127-micron-thick wraparound contacted solar cells, 34-micron-thick sputtered glass covers, and as a substrate a 13-micron-thick polyimide film clad with a copper printed circuit. Each component displayed weaknesses. The thin solar cells had excessive breakage losses. Sputtered glass cover adhesion was poor, and the covered cell was weaker than the cell uncovered. Thermal stresses caused some cell delamination from the model solar array substrate.

A Lightweight Solar Array Study

I. Introduction

Successful rigid substrate solar cell arrays of many designs have flown for some time. However, a new array technology may have to replace the simple theme and variation of past array designs if the larger electrical requirements of currently proposed spacecraft are to be fulfilled. The electrical conversion requirements of most past spacecraft were modest compared to some that are planned, and the simple scale up of conventional rigid arrays proves inadequate. The resultant designs are unacceptably heavy and they require launch stowage volumes that uncomfortably crowd the spacecraft payload. Lightweight fold out or roll out extendable arrays appear promising solutions for the larger electrical photovoltaic converters, and this JPL study examines a lightweight flexible solar array design typical of one for use on a flexible extendable array.

The main thrust of this investigation is directed toward the problems associated with extreme lightweight arrays and with some presently available lightweight components. It would be fortuitous should the minimum weight array design selected for examination prove ideal for use in a flexible array. The theme of this report is not to develop the definitive design, but to record the problems associated with the assembly, and the performance of a lightweight array and its components. The goal of the report is to provide aid to the designer in the selection of lightweight array components and to provide

technical information for more meaningful specifications, inspection, and tests for these.

Discussed in a preliminary manner in the following second section is the selection of the model array module components before their assembly and test: the cell, the cover glass; cover glass processes, and substrate. The third section reports upon the model array module design, assembly, and performance tests, upon the properties of the sputtered glass, and upon the mechanical and electrical changes imparted to the cell by the sputtered cover.

II. Materials and Processes

A preliminary review is made in this section of the components and processes used in the model array module assembly, and the rationale for their selection.

The solar cells were manufactured by Ferranti Limited, Oldham, England. Some of the cells were processed for integral covers by Electrical Research Association (ERA) of Surrey, England, and some were processed by the Ion Physics Corporation (IPC), Burlington, Massachusetts. Simulation Physics Incorporated, Burlington, Massachusetts, attempted to fuse covers on some of the Ferranti cells. The copper clad polyimide flexible substrate was manufactured by the Rogers Corporation of Chandler, Arizona.

A. The Ferranti Solar Cell

1. General. Ferranti solar cells Model ZMS 050224 FW were used in this study. These were N on P 2×2-cm cells, 127 microns (5 mils) thick, that were manufactured of float-zone silicon boron doped to a base resistivity of about 2 ohm-centimeters. Experimental patches of Ferranti cells similar to those used in this study have flown on the earth orbiter Prospero. Ferranti cells of greater thickness have powered a number of European spacecraft including Black Arrow X3 and X4, UK 4 and 5, ESRO, and Intelstat IV.

Being only 127 microns thick, the Ferranti cells offered major weight savings for an array, as did their wraparound contacts that eliminated cell-to-cell metallic ribbon interconnects. The cell solder connection to the printed circuit is the sole cell-to-substrate mechanical bond, eliminating the weight of an adhesive.

2. Ferranti cell contact

a. Wraparound design. The contact design is wraparound with both cell solder contacts on its rear surface. A 24-finger grid is the only contact feature on the active surface of the cell. Each grid finger traverses the top surface and wraps about one edge of the cell to connect to the N contact bar beneath. See Fig. 1. A dielectric applied to this one edge prevents the grids from shorting to the cell's base material. An unplated silicon gap of about 1.5 mm on the rear surface separates the negative from the positive contact areas.

b. The contact conductor. Ferranti used a complex nickel-copper-nickel-gold layered conductor for their contact. The goal was to obtain a corrosion-free electrical contact with good silicon adhesion and good solderability.

A layer of boron-dopped electroless nickel was first deposited upon the base region of the cell. Another layer of differently doped electroless nickel was then applied as a second layer upon the base region and also upon a grid pattern on the active surface; the grid pattern was deposited by a photoresistive technique. A thin layer of copper was then electroplated upon the active and base surface coatings. After a thin layer of electronickel was deposited upon the copper, a thin layer of gold was deposited on the total contact system.

c. Wraparound contact advantages. The wraparound contact offers several advantages to the array assembly:

(1) Cover glass application is simplified in the absence of a top contact to be soldered.

(2) Soldering is upon one array surface, simplifying both array assembly and repair.
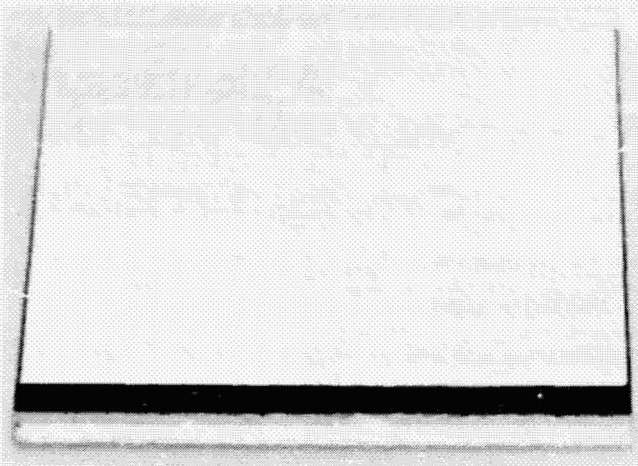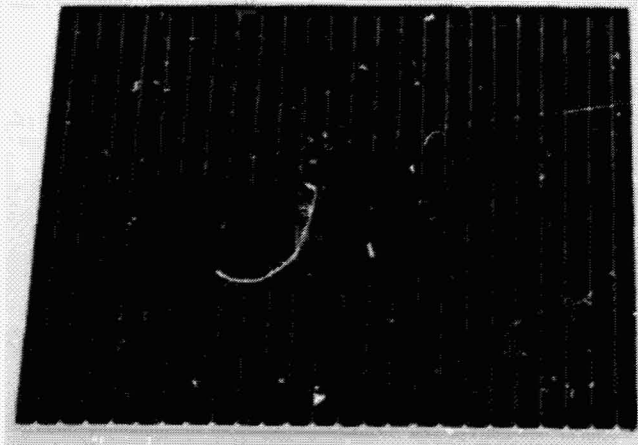
Fig. 1. Ferranti solar cell Model ZMS050224 FW with wraparound contact. The wraparound edge is toward the reader. The negative contact is the narrow strip on the reverse surface; the larger area is the positive contact. The two contact areas are isolated by an unmetallized silicon strip 1.5 mm wide.

(3) The elimination of top-side thermal stress relief looped cell interconnectors eliminates a source of array shadowing when the array is misoriented from the sun in space operations.

B. The Solar Cell Cover Glass

1. General. Cover glass is used to improve solar cell performance. The emissivity of the cover system reduces the solar cell temperature to levels favorable to its operation. Covers also reduce cell damage from radiation and small particles in space. Ideally, the cover glass system is transparent to light flux wavelengths that the cell efficiently converts to electrical energy, and it is opaque to those that limit its performance, such as those UV wavelengths that darken the

cover bonding adhesive. In actuality, light spectra favorable to cell operation suffers transmission loss in the glass, optical coatings, and adhesive. Cover glass system success is gauged upon estimates of the extent to which it protects or enhances cell performance in a mission environment, compared to the estimate of the cell performance without the cover.

2. Cementless cell covers. Applied directly to the silicon surface of the cell, these covers eliminate the bonding adhesive, and the problems of the adhesive application, discoloration, and weight. The process is labor saving, and without the need to protect the cell bonding adhesive, the UV cutoff optical coating could also be eliminated with an opportunity for performance efficiency improvement for those cells sensitive to these wavelengths. The wraparound contact configuration and the sputtered cover process are mutually beneficial. The wraparound design presents no active surface contact to be soldered that must be protected during the covering process. Also, the performance of an integrally covered cell will not be affected as it could with occasional discrete cover misalignment. Such misalignment permits a magnitude of solar cell radiation damage and degradation in space operations that is far in excess of the small percentage of silicon area exposed. Sputtered glass film also deposits upon and protects the cell edges.

No solar cell integral cover has qualified for space use, but it is also true that the definitive solar cell cover has yet to be found. For our study, the cementless cover appears labor saving and promises weight reduction, and we examined three processes: radio frequency sputtering, high-vacuum ion sputtering, and fused covers. Of interest is the reaction of the Ferranti cell to the cover processes, and the reaction of the covers to tests.

3. Sputtering. Sputtering is a process in which material in the solid phase is dislodged with momentum transfer from particle impact in nuclear collision. With a sputtering target material of glass, the dislodged glass particles can be directed to deposit on objects as a thin glass film, and upon the active surface of solar cells as an integral glass cover. Two sputtering processes were sampled in this JPL study. One process used by the Electrical Research Association (ERA) employs radio frequency (RF) excitation. The other, a sputtering process used by Ion Physics Corporation (IPC), uses an electric arc in high vacuum for excitation. Argon ions were used by both processes as the sputtering media. Ferranti solar cells procured by JPL were supplied to these companies to be integrally covered with Dow Corning 7070.

a. Radio frequency sputtering. The process used by ERA is essentially at room temperature, in moderate vacuum, and with an inert argon atmosphere at 0.667 N/m^2 (5 $\times$ 10^{-3}
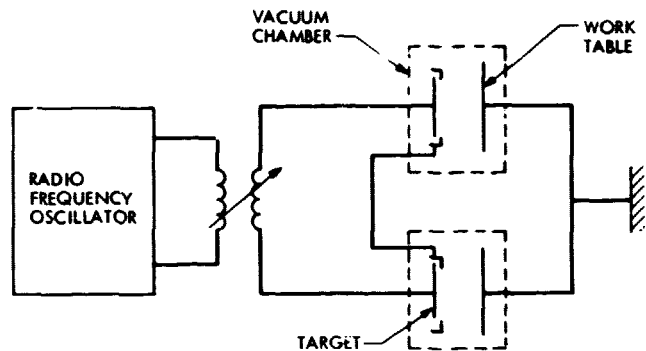
Fig. 2. Schematic of the ERA two-diode sputtering process (from Ref. 1)

torr)[1] as the support gas Excited by the radio frequency field, the argon converts to an ion plasma that strikes the glass target and dislodges glass particles from its surface. The glass particles then deposits upon the solar cell surface. A schematic of the ERA sputtering arrangement is seen in Fig. 2. The equipment has two vacuum chambers, each with a diode and a bulk glass target that is located 4 cm from the work table upon which the cells are mounted (Fig. 3). Individual axial magnetic fields confine the plasma flux to the targets and work tables, both of which are water cooled. The maximum input power is 5.0 kW, 2.5 kW per chamber; however, it was found best to operate a Dow Corning 7070 target at an input power level of about 5 w/cm^2, 3140 watts total, to avoid its fracture.[1] The temperature on the front face of the target rises at a rate of over $100°C$ per power increase of 1 W/cm^2,[2] and there is a temperature difference of about $500°C$ between target faces.[3] The DC 7070 targets are 20 cm in diameter and 3.2 mm thick. The work table diameter is also 20 cm.

The system uses a self-excited push-pull radio frequency power oscillator with a balanced output about ground. It has a tuned anode and a tuned grid with a transformer output. The oscillator is free running at a natural frequency of 13.56 MHz, which changes slightly with the load being driven in the two sputtering chambers. The chambers are also balanced about ground.

The bulk target material is at negative potential and the argon ion flux is positive. Sputtering would cease if the ion bombardment of the surface of the target causes it to assume a positive charge that repels further ion flow. With the electric field reversing however, the target surface receives positive ions and electrons in alternate half cycles at radio frequency. The process is continuous because electron mobility in the plasma is much greater that that of the ions and the bulk target assumes a mean negative potential with respect to the plasma. The ions then move independently of the alternating field as the induced negative potential of the target is seen to be

3

Fig. 3. Detail of an ERA sputtering chamber (from Ref. 5)

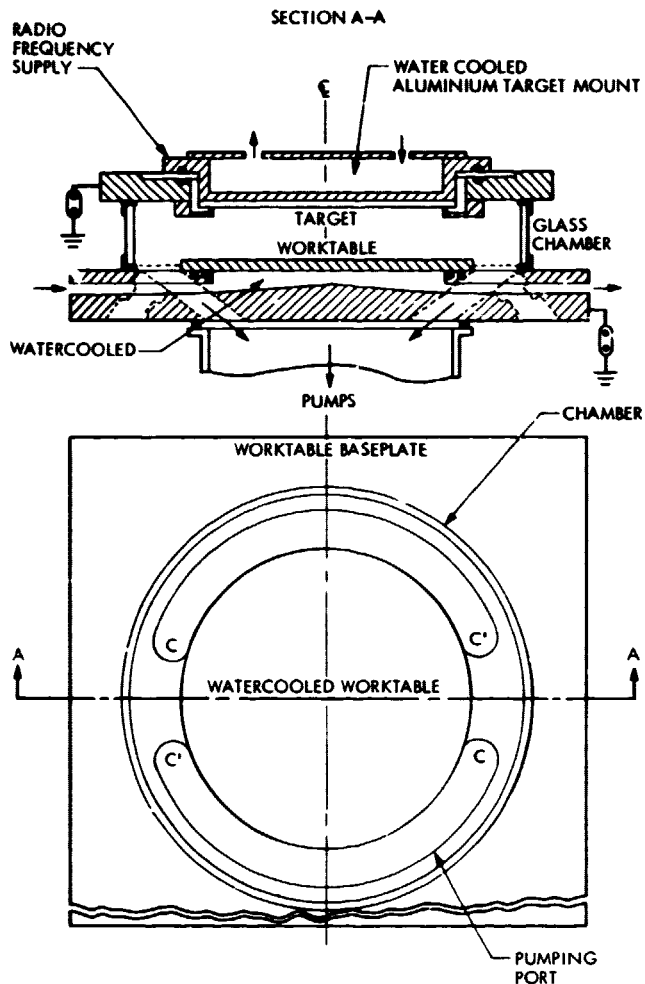Fig. 4. RF sputtering deposition uniformity in prototype unit. Target diameter, 19.5 cm; magnetic field 0.01 W/B/m² (from Ref. 1)
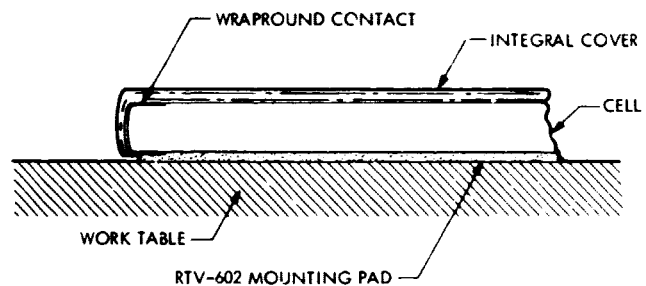
Fig. 5. Mounting wraparound contact cells on RF sputtering work table (from Ref. 1)

constant, and they flow as a high-energy ion plasma of several thousand electron volts peak-to-peak[4] to the target. Ion energy is transferred to the target surface at the impact region, primarily by nuclear momentum transfer. Surface material is stripped from the target, and with energy levels of about 20 eV,[2] the dislodged material flows to the surface of the solar cells that are at ground potential at about 25°C.[4]

Deposition rates are about 1.3 microns per hour[3] in a chamber pressured at 0.600 N/m² (4.5 × 10⁻³ torr) with an atmosphere of 99.999% argon. The specified integral cover glass deposition thickness was 30 to 37 microns, with less than ±10% thickness variation on any one cell. A batch of 35 2×2-cm cells was processed at a time in each of the two chambers of the prototype RF equipment. These were located within a limited 175 cm² area of each work table that provided the specified ±10% cell deposition uniformity. Figure 4 shows the distribution of relative sputtered deposit thickness on the 20-cm-diameter work table. The cells are

temporarily attached to the work table with cured RTV 602 silicone prepared in sheets. Cut to size, the RTV 602 patches are self-adhesive and bond the cells to the work table (Fig. 5). The cells are easily removed when the cover deposition is complete and the adhesive protects the cell rear contact area from unwanted sputtered material, although occasionally such deposits do occur (Fig. 6).

b. Ion sputtering. Ion sputtering is a high-vacuum process at about 1.33 N/cm² (10⁻⁶ torr). As in the RF sputtering process, argon ions are used to sputter a bulk glass target, but argon is present in much smaller concentration. A tube angled at about 45 deg with a vacuum chamber wall serves to collimate an argon ion beam aimed at the glass target located upon the chamber floor.

Argon gas is fed in small quantity at the base of the tube where it is ionized by an electric arc discharge. The ionized gas is accelerated from a high positive potential of about 25 kV through an electrode in the tube at ground potential. Past the electrode, the ion flux moves by kinetic energy through the collimating tube and impacts the DC 7070 target causing sputtering.
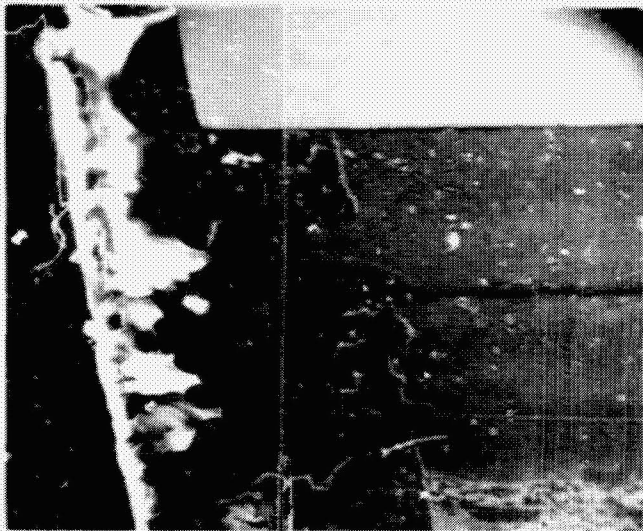
Fig. 6. Undesirable sputtered glass creep onto rear surface of RF sputtered cell; SEM, 150×

Fig. 7. Edge view of bare Ferranti cell presenting its pronounced etched taper; SEM, 65×

The solar cells are mounted on the walls of the chamber above the level of the target plate, an arrangement that keeps the cells out of range of the ion gun. The sputtered glass film deposits everywhere in the chamber, with the deposit rate upon the cells depending upon the current density of the ion beam and the cell proximity to the target. The typical ion sputtering deposition rate is about 30 microns per day.

4. Fused cover glass. Direct cover glass fusion to the cell surface was another adhesiveless cover bonding method investigated. The process wasn't successful with Ferranti cells. Simulation Physics Incorporated, Burlington, Massachusetts, uses temperatures between 450°C and 500°C and an electro-static field for the fusing process that has been successful in covering a number of cell types. The electrostatic field between coverslip and the silicon surface of the cell imparts about 350-psi pressure upon the cover as the cover and cell are heated. The weight saving with this method is simply that of the omitted cover glass adhesive. Conventional discrete covers are used having thicknesses consistent with space mission requirements and minimize breakage in handling. Direct fusing promises a cover bonding process that is more labor efficient and cost effective than those using adhesives, and a sampling of Ferranti cells were covered to test their compatibility with this fusing process.

DC 7070 covers 25 microns thick that were immediately available were used to test the process, with the intended 150-micron-thick DC 7070 covers to be used on additional cells if the process proved successful. The 450°C temperature was the minimum required to fuse either cover thickness. Two minutes were required for prototype equipment to reach

fusion temperature, and three minutes more were required to soak the covers to complete the fusion of cover to cell.

Both the 24-finger grid and the pronounced etched taper of the Ferranti cell, Fig. 7, impeded proper fusion of cover to cell surface. The process required higher temperature and longer time for the glass to suitably soften and properly drape about the cell structures before fusion. However, the Ferranti cell open circuit voltage had already degraded after exposure to 450°C in the limited time interval that provided inadequate cover fusing conditions, and this covering process was not pursued with the Ferranti cells.

5. Dow Corning 7070. Dow Corning 7070 has a higher coefficient of thermal expansion and significantly lower degree of resistance to thermal shock with respect to silicon than do other members of the borosilicate family of glasses. But in sputtered form, DC 7070 exhibits less intrinsic stress than do other borosilicates. Figure 8 presents the intrinsic stress of sputtered Schott 8330, DC 7740, and DC 7070 borosilicates in comparison with that of sputtered fused silica.

a. Intrinsic stress of sputtered DC 7070. Curvature of cantilevered silicon beam witnesses placed in the sputtering chambers show stress of DC 7070 sputtered deposits at about 2.9×10^7 dynes/cm^2.[5] Beam witnesses were used because of their past utilization as a bent beam for intrinsic film stress analyses.[6]

b. Electron irradiation of sputtered DC 7070. Sputtered DC 7070 exhibited a 3% loss in transmission at 0.400 microns after exposure to 10^{15} electrons/cm^2 at 1 MeV in a sputtered
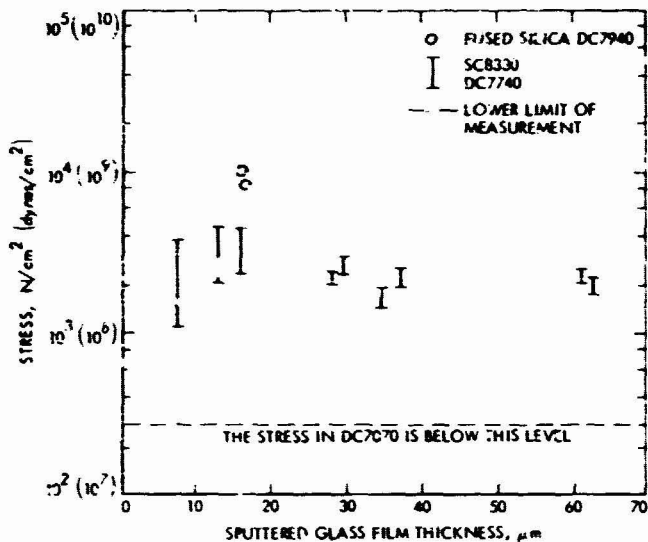
5

Fig. 8. Intrinsic stress as a function of sputtered fused silica and borosilicate glasses of various thickness (from Ref. 1)

Fig. 10. Radiation induced transmission loss in sputtered DC 7070 integral glass cell covers with and without ceria; 10¹⁵ electrons/cm² at MeV (from Ref. 1)

cover 103 microns thick[1] (see Fig. 9). Another similar test on a 50-micron-thick sputtered DC 7070 deposit showed a 1% loss between 400 nm and 1200 nm, and another irradiation test upon DC 7070 sputtered films 20 microns thick showed negligible transmission loss compared with controls.[4] These sputtered deposits were without ceria dopant.

ERA reports no success in reducing radiation induced transmission loss in DC 7070 with the addition of cerium

Fig 9. Sputtered Dow-Corning 7070 irradiated with 10¹⁵ electrons/cm² at MeV (from Ref. 1)

oxide. This dopant has reduced loss in other borosilicates. Ceria dopant levels at 1% to 5% by weight introduced greater transmission loss because of its presence in the sputtered DC 7070 than the subsequent loss from exposure to a fluence of 10¹⁵ electrons/cm² at 1 MeV[1] (see Fig. 10).

c. Antireflective coating on sputtered DC 7070. Sputtered DC 7070 integral covers were deposited upon Ferranti cells that were coated with magnesium fluoride as an antireflective (AR) coating, and the DC 7070 sputtered covers were again coated with a $MgF_2 \lambda/4$ AR coating. Radio frequency sputtered MgF_2 coatings were attempted by ERA, but these unacceptably discolored the cover glass.[7]

C. The Sample Array Module Substrate

Flexible film polyimide was the selected substrate material. This film, R-Flex 8191, manufactured by the Rogers Corporation of Chandler, Arizona, was 13 microns thick and had a copper laminate on one side weighing 153 g/m² (0.5 oz/ft²) that would provide the printed circuit to accommodate the solar cells.

III. Applications, Tests, and Performance

Discussed in this section are the sample array module design, its assembly, and thermal cycle tests. Also in this section, the sputtered glass cover is examined in detail and an evaluation made of the manner in which the cell is mechanically and electrically affected by the cover deposition.

A. The Lightweight Array Design Module

As stated earlier, the prime purpose of this study is to explore the problems associated with an extremely lightweight array design, its components, and assembly. Were this test module model successful, it could be enlarged to appropriate array module size, many modules of which could be assembled into a desired array configuration. An outboard bus wiring system is proposed to facilitate interchangeability and to reduce impediment to array stowage and deployment. With a cable design possessing increasing multiples of parallel connections to modules further outboard on the array, the array modules would have matched impedance, and consequently equal module voltage at the main power bus.[8] Other required components of the lightweight array system, such as the extendable array deploying and flexible substrate tensioning devices, are not addressed in this report.

1. Sample module design. A printed circuit pattern developed by JPL for another 2X2-cm cell wraparound contact application was used for the sample module. It was applied on the R-Flex 8191 polyimide substrate copper laminate surface by a photographic process. The pattern is shown in Fig. 11. The sample array module accommodated 16 solar cells, each cell electrically connected in series and parallel in a four-by-four cell matrix arrangement.

A metal frame was used to support the substrate in tension and was also used to mount insulated binding posts to facilitate electrical measurements.

2. Sample module assembly. Pulsed reflow soldering equipment was used to apply the required heat and pressure to solder the cells to the copper circuitry on the flexible substrate. A frame fixture of welded nickel ribbon held the cells in proper alignment and spacing during the soldering operation. Pressure under the cell was evenly distributed with the use of a soft teflon pad lining on the bottom of the fixture. The pad reduced cell fracturing during assembly. Earlier efforts failed to suitably assemble the module from the rear of the polyimide film using manual soldering techniques. Three frames were assembled, each containing 16 cells from a category: bare, ERA and IPC covered. A cell fragment from each category of cells that were broken during assembly was mounted on the unclad border of the sample module as a site to mount a thermocouple. This thermocouple monitored temperature during the electrical performance and temperature cycle tests that followed.

3. Thermal cycling sample module. The sample modules were electrically tested before, and at intervals during the thermal cycle tests. Simulated AMO 135.3 mW/cm^2 at 28°C were the electrical test conditions. Figure 12 describes the six-minute thermal cycle periods with temperature excursions between -125°C (-193°F) and 80°C (176°F). A dwell of four minutes at the 80°C high temperature level was required after every fifth cycle to replenish the LN$_2$ supply. Each sample module was cycled 900 times. Each string of four paralleled cells was electrically tested in each of the sample modules as the other strings were open circuited. Figure 13 presents the

Fig. 11. Copper printed circuit on sample array module substrate

Fig. 12. Thermal cycle conditions for modal array module

7

Fig. 13. Short circuit current of sample module strings at thermal cycle intervals

Fig. 14. Maximum power of sample module strings at thermal cycle intervals

short-circuit current at thermal cycle test intervals. Figure 14 shows the maximum power levels of the cell strings.

a. Cell delamination from substrate. A total of 12 cell strings started the tests on the three sample modules. Eight strings survived the 900 cycles. Four cells sufficientl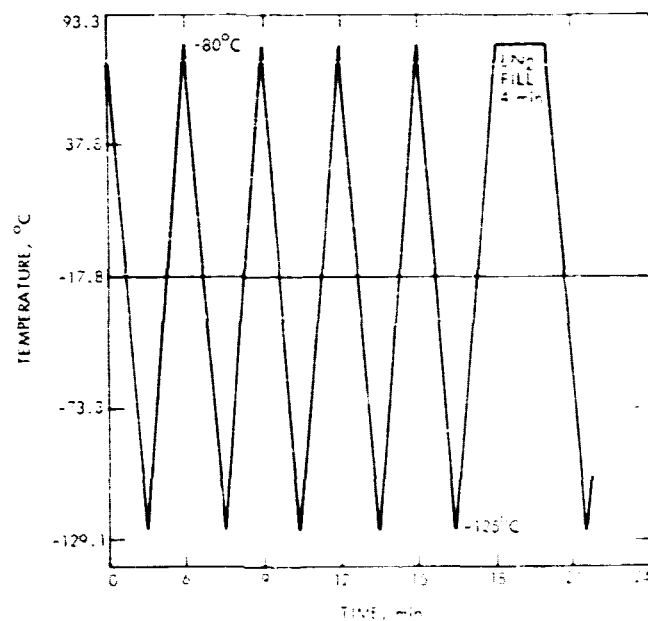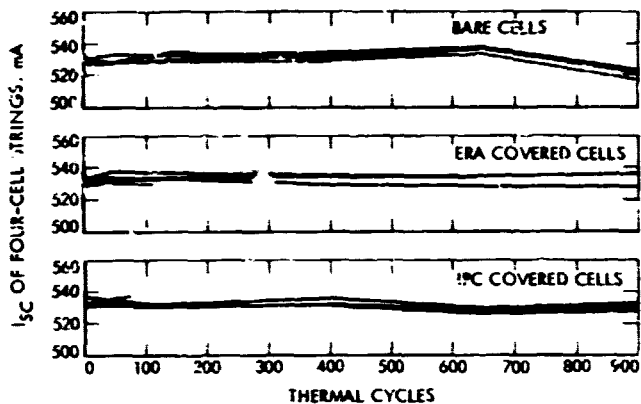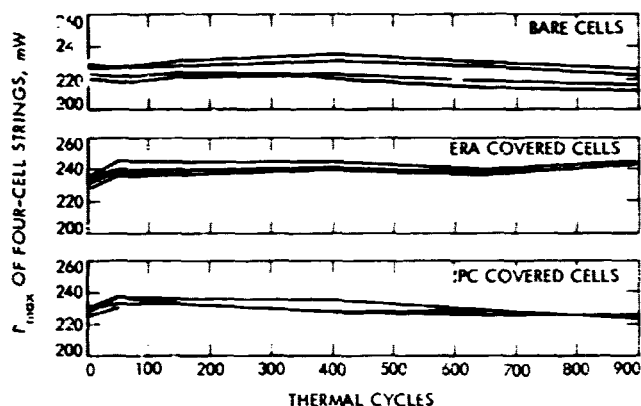y delaminated from the substrate to cease electrical contribution to the circuit. Delaminated were one cell from the bare cell sample module after 650th cycle, one from the ERA integrally covered solar cell module after the 150th cycle and one after the 650th, and one from the IPC integrally covered solar module after the 50th cycle. Affected curves in Figs. 13 and 14 discontinue after the failures.

The cause of the failures is uncertain. The cell-to-printed circuit soldering was an intensive, painstaking custom effort, rather than one to seek a production line technique. A

production line technique for a similar array application was developed by the Royal Aircraft Establishment, UK, employing hot gas as the soldering heat source,[9] equipment JPL lacked. Custom soldering is no guarantee of success, and soldering weakness could contribute to the thermal cycling failures, particularly the failures early in the test. However, the failures later in the test could be attributed to the basic lack of thermal stress relief between the cell and the substrate's printed circuit.

b. Cover delamination due to thermal cycling. Figure 15 displays photographs of the sample modules at intervals during the test to the 650th cycle. Photos after the 900th cycle lacked additional information and were omitted. Dark images seen in the prethermal cycle photos were of camera structures, images that were eliminated from subsequent photos. Changes in the appearance of the integral cover glass indicate progressive cover delamination with thermal cycling.

The delamination takes two forms. One form shown is the small spots seen in quantity on some ERA processed cells, which, unseen in the photos, are mirror-like in quality. Delamination is also seen as bubbles. Both spots and bubbles are indicators of cover delamination at different AR coating levels. The spots are flecks of magnesium fluoride reflective coating that adhered to the under-surface of the integral cover as the AR coating delaminated from the silicon surface of the cell. The bubbles are areas where the integral cover delaminated from the upper surface of the AR coating.

Delamination from both levels are seen on ERA coated cells. Only delamination of the sputtered cover from the AR coating is indicated on IPC cells, but most of the bubbles on the IPC cells appear to have grown during the thermal cycling from smaller bubbles existent before the test started. Since random AR coated Ferranti cells were submitted to both firms for covering, it would appear that the manner of delamination and its relative severity are due to the different sputtering processes.

Judging from the results of materials and techniques used in this study, sputtered integral cover adhesion to cells on arrays in storage is questionable for IPC covered cells, and questionable in thermal cycling for both processes. See the discussion in Subparagraph II-B-6 of sputtered cover delamination occurring after another test having wide temperature range.

B. The Sputtered Glass Solar Cell Integral Cover

Examined in this subsection are the special requirements for solar cells that are to be processed for integral covers, some sputtered glass properties, and the mechanical and electrical changes in a cell after integral cover deposition.

Sputtered glass film properties are similar to the original bulk target material from which the deposit was derived. This could be expected since the processes lack phase change, such as thermal evaporation and condensation. However, while the glass properties are similar they are not exactly the same, because the sputtered glass film is the product of reassembled atomic and molecular units from the starting material, and changes do occur between the original and sputtered glass. Some of these should be noted when the glass film application is a solar cell cover. Figure 16 is a scanning electron microscope photograph of the cross section of a sputter covered Ferranti solar cell. Note the cell's bottom contact, cross section of a grid finger, and the outline of the sputtered film deposit.

1. **Solar cell features and the integral cover.** If solar cell costs are to be reasonable, so must be their specifications. Solar cell applications often permit some superficial mechanical defects without sacrifice to system operation, and cell specifications often sanction these in the interest of improving production yield. However, edge chips, irregular edges, and other minor flaws normally considered cosmetic blemishes, are serious defects for cells to be integrally covered, since intrinsic stress within the cover that is imparted to the cell promotes the possibility of cell breakage starting at such defect sites.[10]

If defect-free solar cells are available, they probably would be at a cost premium that impacts the possible cost savings of this cell cover technique.

Sharp cell edges result in highly stressed areas for the integral cover. Cracks at the edges, or incomplete glass coverage, could start cover delamination.[10] At an edge of a Ferranti cell grid finger in Fig. 17 is a stressed area in an ERA deposited cover in which a crack is seen that was typical of cracks found at many grid finger edges displayed under the scanning electron microscope.

Such cracks can propagate in size and number with handling, array tests, launch, array deployment, and thermal stresses in space operation.

2. **Properties of the sputtered glass cover**

a. *Stress.* Pure silica makes an excellent solar cell cover. It has a high sputtering rate, high thermal conductivity, low thermal expansion coefficient, low dielectric loss, excellent resistance to radiation induced darkening, high optical transmittance, and moderate cost. Its major handicap for this application is the high level of intrinsic stress that it generates within its sputtered film growth. The stress is great enough to delaminate the integral cover from the cell surface, or fracture

the cell.[1] Stress measured as high as 10^4 N (10^9 dynes)/cm² make impractical deposits on solar cells of pure silica sputtered glass film thicknesses in excess of 25 microns.[4]

Dow Corning 7070, a borosilicate, does not match the favorable characteristics of pure silica as a solar cell cover glass, but its sputtered film grows with much less intrinsic stress. Measured at 2.9×10^2 N (2.9×10^7 dynes)/cm²,[1] the intrinsic stress of sputtered DC 7070 about equals its thermal expansion stress in typical application.

The dominant component of RF sputtered cover stress arises during film growth by not well understood[3] changes in film structure.

For the high-vacuum ion sputtered processed covers, the intrinsic stress is thought to result from several sources:

(1) Thermal mismatch. One cause is thought to arise from an expansion coefficient mismatch between cover glass and silicon, which is not very serious for DC 7070: $3.2 \times 10^{-6}/°C$ vs $2.9 \times 10^{-6}/°C$.[2]

(2) Spreading layers. Each successive glass monolayer deposit is thought to spread because of the impact and partial imbedding of subsequent sputtered material. The resultant spreading of layers is believed a stress cause.

(3) Hydrophilic nature. The hydrophilic nature of sputtered glass is another possible stress cause; both the glass and the process technique are believed to contribute. Sputtered pure silica glass covered solar cells that appeared normal when viewed through a vacuum chamber port have bowed and fractured when brought to atmospheric pressure levels. Simple tests isolated the source of the dramatic stress increase to the water vapor in the atmosphere.

For most glasses tested, the thermal expansion component in the sputtered integral cover appears subsidiary to its intrinsic stresses.[1] Annealing a sputtered silica cover free of its high intrinsic stress is unsuccessful because its high softening temperature degrades the solar cell junction. Complex silica based glasses generally have poorer properties for cell covers than pure silica, but they have lower softening temperatures that could lead to a successful anneal of a cover. One, DC 7070, generated sputtered glass film of unusually low intrinsic stress, a major advantage when the application is a sputtered cover on a solar cell.

SAMPLE
ARRAY
MODULE
WITH
BARE
CELLS
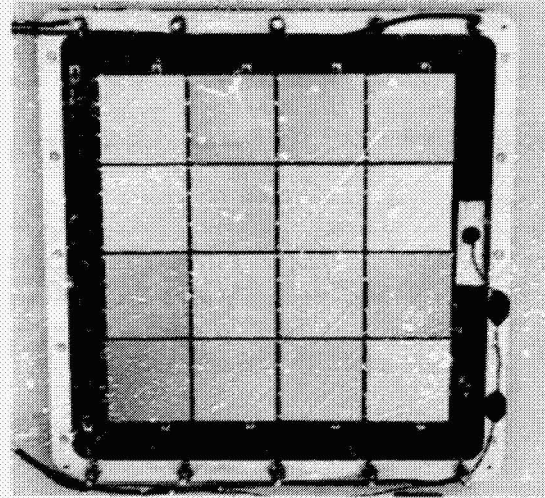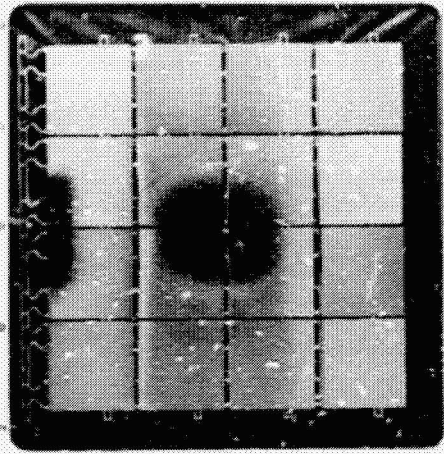
SAMPLE
ARRAY
MODULE
WITH
ERA
COVERED
CELLS
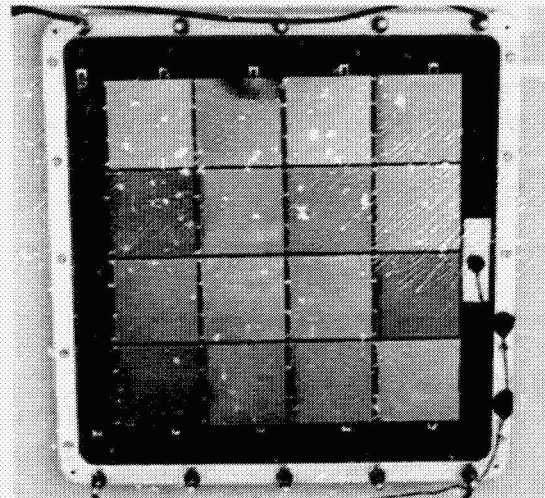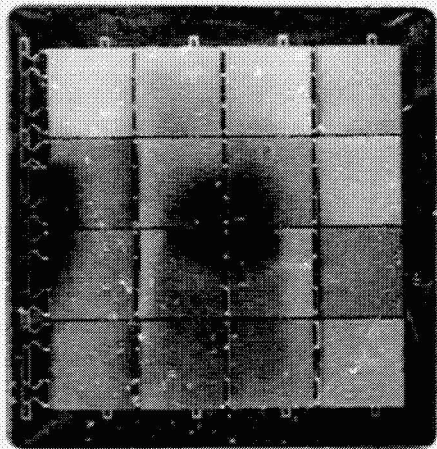
SAMPLE
ARRAY
MODULE
WITH IPC
COVERED
CELLS
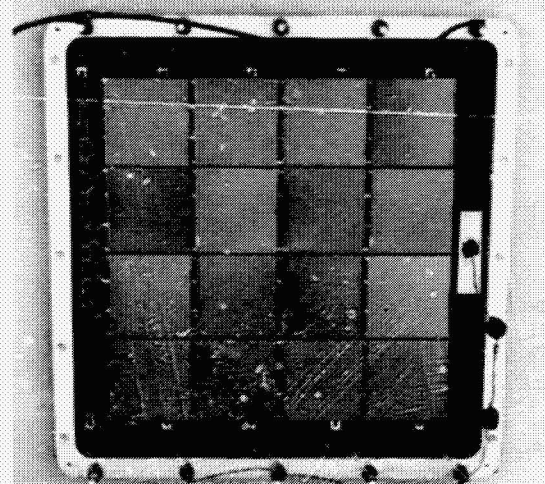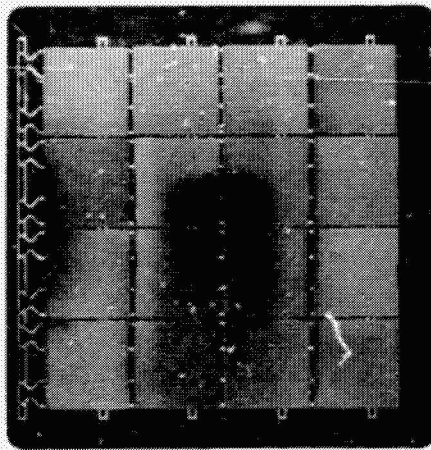
BEFORE START OF THERMAL CYCLING

150 CYCLES

SAMPLE ARRAY MODULE WITH BARE CELLS
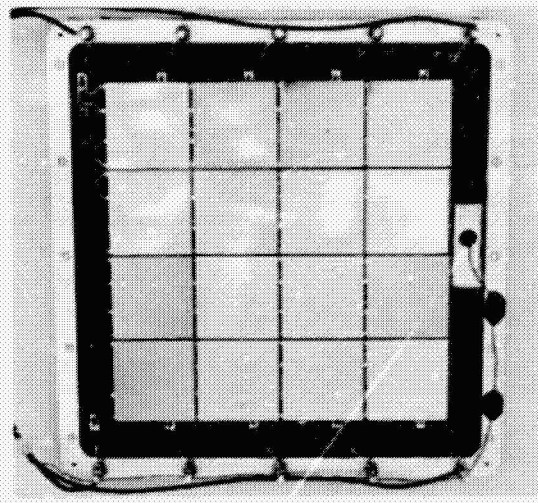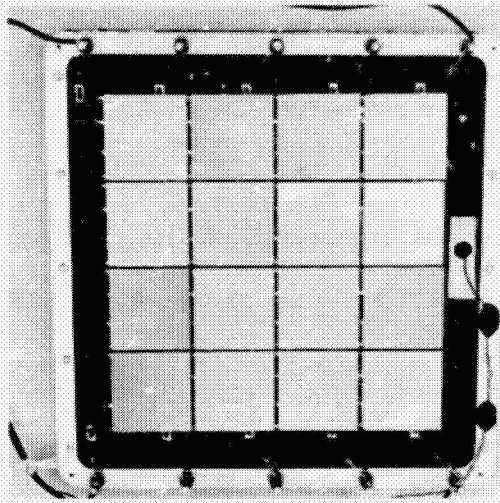
SAMPLE ARRAY MODULE WITH ERA COVERED CELLS
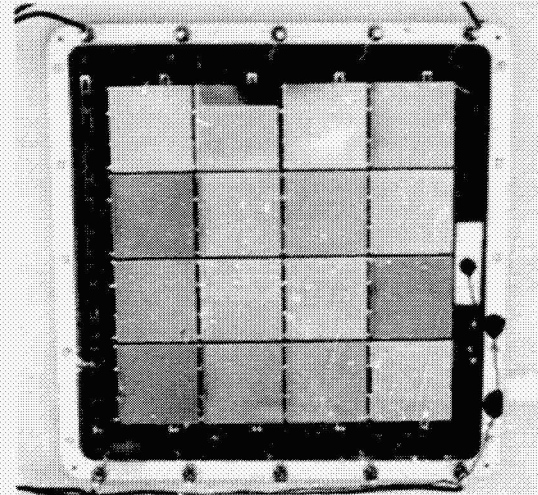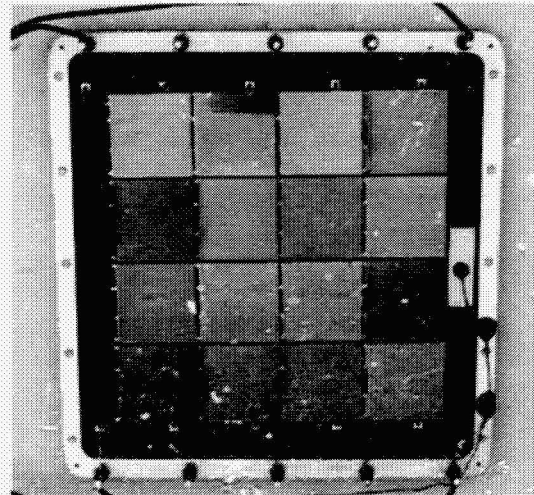
SAMPLE ARRAY MODULE WITH IPC COVERED CELLS
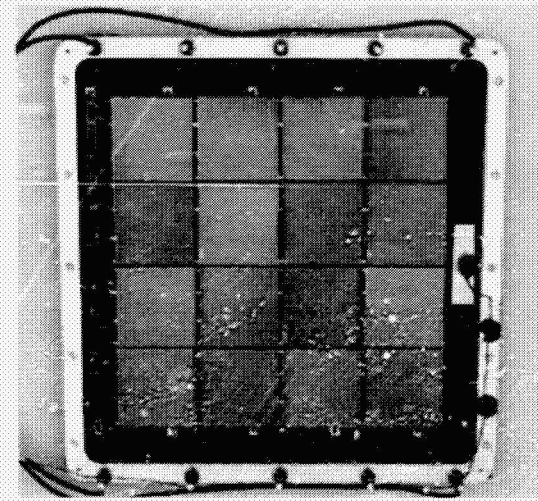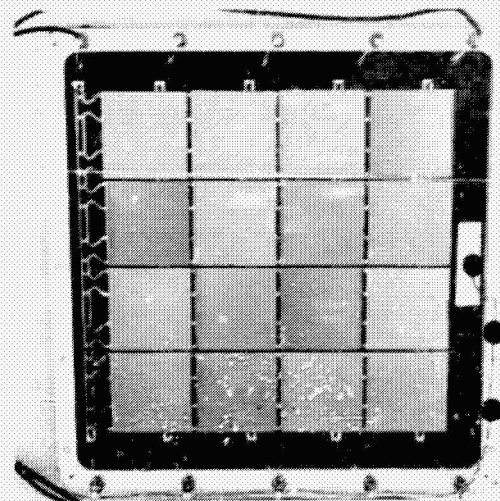
400 CYCLES

650 CYCLES

Fig. 15. Sample array module photos at thermal cycle intervals. Note cover delamination (see Subparagraph III-A-3-b) as test progressed
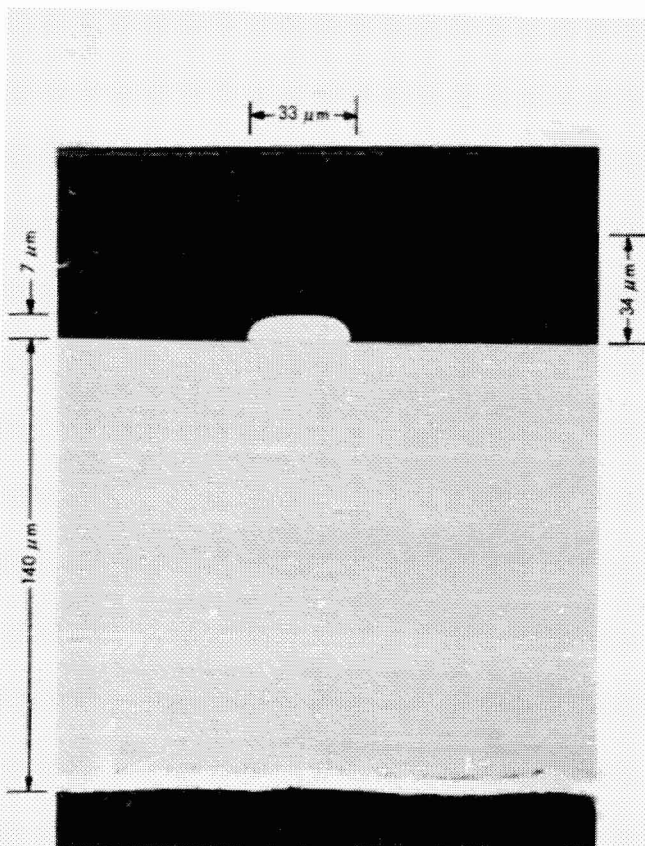
Fig. 16. Cross section of Ferranti cell with integral cover glass sputtered by Ion Physics Incorporated; SEM, 500×
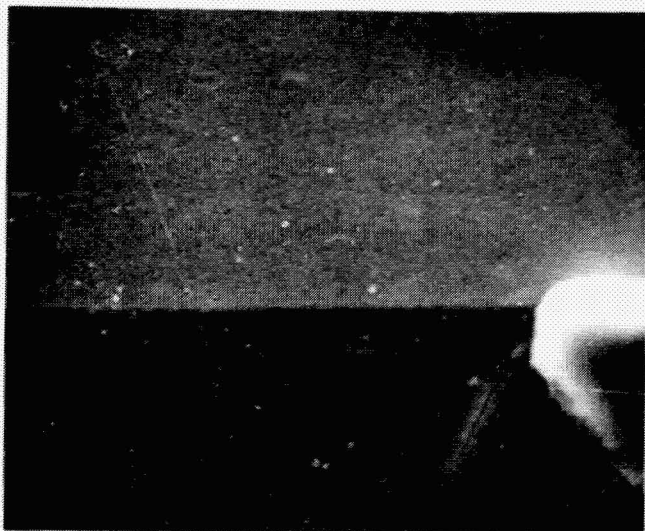
Fig. 17. Crack in integral cover at edge of grid finger; SEM, 4600×

It is risky to further stress so brittle a material as silicon. Considering the dependence of a spacecraft upon its power source, the prudent array designer would want prior tradeoff studies and firm technical evidence of superiority of any new

process or material that is associated with stress increase to the solar cell. The evaluation would include tests of integrally covered cells that simulate launch vibration and acoustic stresses and stresses associated with temperature extremes and thermal cycling in the space environment.

b. Integral cover adhesion. Since the Ferranti cells possessed a magnesium fluoride antireflection coating, the adhesion in question in this investigation is that of the integral glass cover to this coating. Sputtered glass coatings have adhered poorly to cerium dioxide AR coating.[4] In the RF sputtering process, the AR coating serves as a shield against possible cell damage resulting from the argon ion flux.

In question in this study is how well will the sputtered covers adhere to the cells in storage, thermal cycling, and temperature extremes. From test evidence of the cover processes examined, Subparagraphs III-A-3-b and III-B-6, the prognosis is poor for the three conditions.

c. Optical quality of the sputtered cover. The optical quality of the sputtered cover is not that of its bulk counterpart. Grown in layers with bond angles unlike the original glass, the sputtered glass film is not optically flat and is more poorly structured.[11]

The lack of optically flat solar cell covers will influence array output in off-sun array operations in flight. Except at extreme angles, the output of most solar arrays with conventional covers that are maneuvered off the sun is a function of the cosine law, ignoring shadowing. If the power output of an array with sputtered covers falls off much more than could be expected by the cosine function after moderate sun misorientation, this deficiency may have to be adjusted in some missions by appropriate array overdesign.

A comparison is shown in Fig. 18 of light transmission through a bare Dow Corning 0211 substrate 500 microns
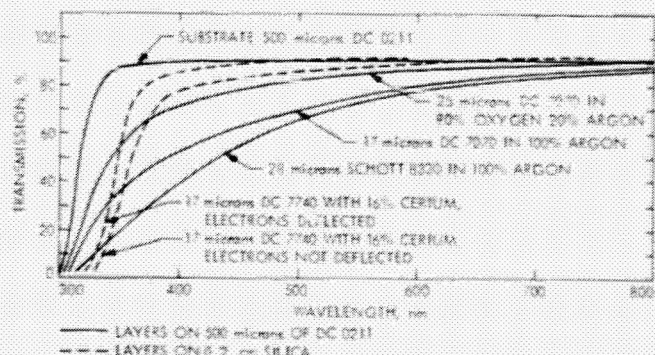
Fig. 18. Light transmission of sputtered glass deposits (from Ref. 2)

thick, and through RF sputtered glass deposits upon this substrate.[2] Compared are sputtered borosilicate glass coatings of DC 7070 in an atmosphere of 100% argon, 80% oxygen, and 20% argon, and also Schott 8330 in 100% argon. Transmissibility of DC 7070 is seen superior to that of Schott 8330. Although the 80% O_2 - 20% Ar atmosphere improved DC 7070 transmissibility, it impaired the sputtering deposition rate and subsequent cell performance because the cell contacts reacted to the oxygen. RF sputtering in 20% oxygen showed no improvement.[2]

d. *Absorptance coefficient.* The absorptance coefficient is high.. in the RF sputtered glass deposit than in   .other bulk material. The typical increase is between 2 to   nt at 400 nanometers. The resultant power loss is about 1..% with an absorptance coefficient loss of 3% at 400 nanometers in AMO sunlight.[1]

e. *Density of the sputtered glass film.* Density changes of the sputtered glass film from that of the bulk source indicate problems. Density reduction signals deposit porosity or voids within layers with consequent diminished protection for the cell and questionable cover stability. Increased density indicates an out-of-control sputtering process. Specific gravity bottle measurements[1] indicated the RF sputtered glass to be 2.22 ±0.02 g/cc compared to 2.13 g/cc of the parent material. The 5% density increase is considered insignificant with respect to cover glass performance, but it adds to array weight.

f. *Argon inclusion.* With RF sputtering, argon becomes incorporated in the sputtered glass film. Concentration is about 1% by weight of the sputtered deposit.[1] Argon inclusion in the glass deposition is not reported for the high vacuum ion sputtering, and the small concentration of argon present in this process should not make it much of a problem.

Argon outgassing in space vacuum conditions is a concern because of the possible effect upon the mechanical integrity of the sputtered cover.

g. *Undesired sputtered deposits.* Debris occasionally sheds from the sputtering chamber structures and deposits upon the integral cover film. Figure 19 is a scanning electron microscope photograph of such deposits; the diagonal structure is a grid finger 33 microns wide. Prototype sputtering equipment used at ERA included a portion of the chamber floor as the work table upon which the cells were processed. To reduce debris, RF sputtering production equipment will be designed with the work table as the chamber ceiling. Some IPC processed cells also exhibited these debris deposits.

At sufficient solar intensity in space, debris deposits can become damaging solar flux concentrators. The thermal
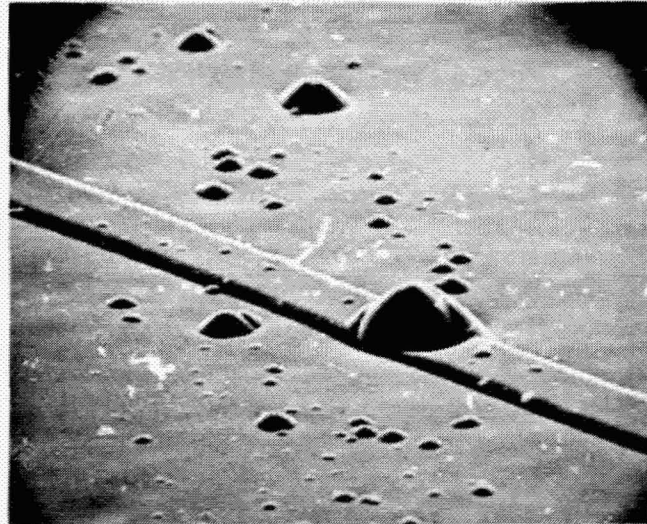
Fig. 19. Undesirable chamber debris deposits on integral cover; SEM, 350×; diagonal structure is a grid line 33 microns wide

gradients they create could cause injurious silicon thermal stress, or they could become locales of cover delamination.

h. *Possible solar cell damage during sputtering.* Both argon ion and electron fluxes reach the cells in RF sputtering. The argon ion flux could damage the surface of the cells. Excessive cell heating because of electron bombardment can damage the cells,[5] and can also darken the deposited glass cover (see next sub-paragraph). As the argon ions ablate the glass target, they also erode the integral cover deposited upon the solar cell, at a slower rate than that of the deposition.[3]

The AR coating shields the solar cell from ion flux damage.[3] For cells without an AR coating, solar cell junction damage can be avoided in the RF sputtering process if the power density at the cells is reduced below 0.6 W/cm^2 for the first 200Å of the sputtered film deposit (from IBM patent 1145348 cited in Ref. 12). Axial magnetic fields to divert the electron flux from the cells, and watercooled chamber structures, have reduced cell temperatures during the RF sputtering process.

Solar cells to be integrally covered appear less vulnerable to damage with high-vacuum ion sputtering than with the RF sputtering process that will require careful process management.

i. *Discoloration of sputtered film.* Borosilicate sputtered glass films have darkened because of the electron flux present in the RF chamber plasma. Electron fluence is estimated at 10^{16}/cm^2 per glass film monolayer deposited; each successive film layer is fully exposed to this electron flux for a total of

10^{21}/cm^2 on a 100-micron thick film.[3] The power density at the area where the cells are RF processed is about 0.80 W/cm^2 [1] for a 1.3-micron per hour deposition rate. Electrons impact the cells with about 20 eV of energy.[2]

Darkening was reduced in an atmosphere of 80% oxygen - 20% argon, but these conditions created other problems (Subparagraph III-B-2-c). Darkening was further reduced at the RF process work table with magnetic fields used to divert the electron flux from the cells (Fig. 18), but the field alters deposition uniformity and permits fewer cells at a time to be processed. Ceria doping at concentrations from 1% to 5% by weight have not reduced borosilicate glass darkening in the RF process; instead, the transmission loss due to the ceria addition was greater than the resultant darkening of undoped glass exposed to 10^{15} electrons/cm^2 at 1 MeV electrons[1] (see Fig. 10).

The RF sputtering plasma is seen to have an electron flux component, that could darken the cover glass, which is more severe than that impacting spacecraft solar arrays during many space missions. The sputtered cell cover glass is exposed to a less damaging environment in the high-vacuum ion sputtering process.

Darkening of glass film in the high vacuum ion sputtering process is thought due to chemical reduction of the target material because of the argon ion flux.[2] With the removal of alkalide oxides from the glass, areas of silicon darkened the glass deposit. The stoichiometric change causing the glass darkening was diminished in the ion sputtering process by first evacuating the chamber to 1.33×10^{-1} N/cm^2 (10^{-7} torr) and back filling with oxygen to 1.33 N/cm^2 (10^{-6} torr). Cell contacts were not affected with this procedure.

j. Carrot defects. All sputtered glass films exhibit defects called carrots.[1] These are seen in the film as small round bubble structures of various sizes and population densities; they are brightly visible when the sputtered glass film is illuminated against a darker background (See Fig. 20). The defects appear to increase with the argon pressure within the RF sputtering chamber, possibly with increased inclusion of argon within the growing film.[1] More intensive cell surface cleaning appears to have little influence upon inhibiting their growth. The carrot defects appear most directly related to roughness of the cell silicon surface or to slight protrusions above its plane. Pits in the cell surface create no carrots.[3] With the RF process, the best quality covers are deposited on cells having highly polished flat surfaces.

Figure 21 is a sketch of a carrot. In any stage of the glass film deposit, the height of the carrot above the film plane is the height of the protrusion above the cell surface. In the cross

Fig. 20. The bright objects are carrot defects; SEM, 670×. Etched patterns on the solar cell surface are the larger features (from Ref. 3)
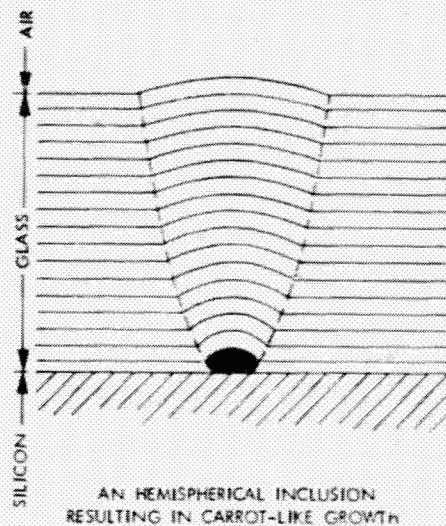
AN HEMISPHERICAL INCLUSION
RESULTING IN CARROT-LIKE GROWTH

Fig. 21. Sketch of carrot growth in sputtered glass (from Ref. 2)

section of a Ferranti cell with an integral cover shown in Fig. 16, the glass deposit also appears to follow the contour of the grid finger below. Figures 22 through 24 present additional views of carrot formation.

Carrot deposits also appear capable of acting as miniature solar flux concentrators, as were the debris deposits from the chamber (Subparagraph III-B-2-g). With sufficiently high solar intensity levels, these also could cause damaging silicon stresses or start cover delamination. Also of concern is the preferential fracturing about similar defects in sputtered glass solar cell covers that has been reported.[13]

Fig. 22. Optical phase contrast micrograph of carrot growth in a cleaved edge of RF sputtered glass; 550× (from Ref. 2)

Model 701-5P050-1 two axes digital micrometer with microscopic optical alignment with an accuracy of ±1.27 microns was the measuring instrument. The total population of Ferranti bare and IPC and ERA covered cells for this measurement numbered 153. Dimension averages of the processed cells are compared to the dimension average of the unprocessed bare cell in Table 1. This dimension specification for the bare Ferranti cell had been: length = width = 20.02 ±0.1 mm.

Table 1. Changes in length and width of a sputtered cell

Group	Average length mm	Change		Average width, mm	Change	
		μm	%		μm	%
Bare	20.0299	–	–	20.0421	–	–
ERA	20.0396	+9.7	+0.05	20.1678	+125.7	+0.63
IPC	20.0609	+31.0	+0.15	20.0652	+23.1	+0.12

Fig. 23. Carrot defects at a fractured sputtered film edge; SEM, 1540× (from Ref. 3)

3. Mechanical changes in cell due to integral cover deposition. Changes in cell mechanical characteristics due to the integral cover deposit are reviewed in this section.

a. Change in cell length and width. Cell length and width dimensions change, as well as thickness, since about 40% of the depth of the glass film deposited upon the cell active surface also deposits upon the cell edges.[4] An Autometrics

Fig. 24. Top of a carrot defect on RF sputtered DC 7070 film; SEM, 1540× (from Ref. 2)

b. Change in cell thickness. A Microsense 3046A determined the cell thickness by means of opposing capacitively coupled probes. The instrument minimized handling of the fragile cells. Four measurements were recorded on each cell with a probe having a 317.5-micron (0.125-inch) diameter.

Table 2. Thickness of cell and sputtered integral cover

Group	Quantity of cells measured	Mean cell thickness, μm			Mean cover thickness, μm		
		Min[a]	Nominal	High	Min	Nominal	High
Bare	70	128.0	149.9 ±0.74	163.6	–	–	–
ERA	65	157.1	172.5 ±0.74	194.7	4.8	29.6	41.8
IPC	75	154.6	166.4 ±0.51	193.4	11.1	23.5	36.0

[a]One probe on bare silicon between positive and negative contacts.

The thickness measurements were averaged for each cell. The thickness measurement of the bare cell included a grid finger, but this 7-micron thick structure is included within the glass film deposit. Accordingly, the integral cover thickness is the difference between the two measurements plus 7 microns; these thicknesses are presented in Table 2. The specified Ferranti cell thickness is 127 ±25 microns. The specified cover is 30 to 37 microns thick.

c. Cell bowing. The bare Ferranti cell bows because of intrinsic stresses within its silicon wafer, from its contacts, and from solar cell manufacturing processes. The sputtered glass film adds complex stresses of its own to complex stresses that already exist in the cell, and bowing of the covered cell reflects the resultant of these stresses in equilibrium.

A datum plane is established at each cell low point, and cell bowing above this plane is measured as the instrument probe of the Microsense 3046A, operating in a mode to detect thin wafer bowing, is walked across the paths with respect to the reverse side of the cell as shown in Fig. 25. Measurements were taken active side up. The bowing data is shown in Table 3.
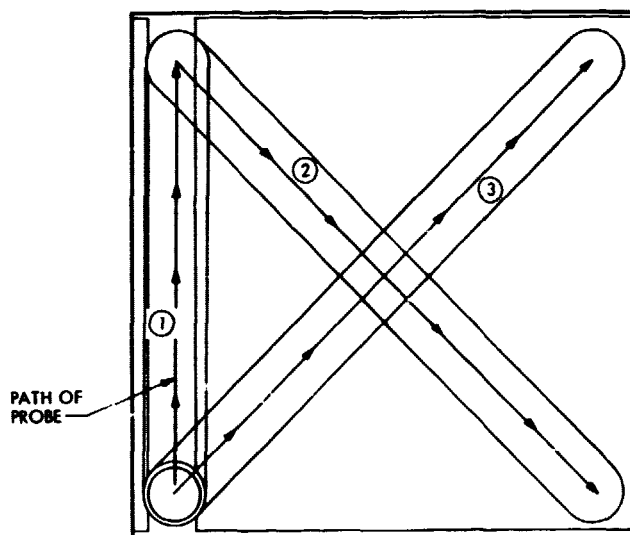
Fig. 25. Paths on Ferranti cell along which bowing data was taken

Table 3. Maximum cell bowing along paths shown in Fig. 25

Group	Quantity of cells measured	Average cell bow, μm		
		Edge	Diagonal 2	Diagonal 3
Bare	21	30.0	30.0	31.0
ERA	18	39.4	50.8	51.3
IPC	27	54.1	80.5	81.8

d. Cell strength of material. The purpose of these tests was to determine quantitatively the basic strength of this Ferranti

127-micron cell and how its strength was altered by the cover depositions.

The tests were performed as they were in a previous JPL study,[14] and procedures were in accordance with Federal Test Standard 406, Method 1031. The same three-point cell loading test fixture was used (see Fig. 26). Tests were performed at room temperature with an Instron testing machine. Cell deflection to failure under load was recorded as was the cell breaking force. Data analysis was simplified with the covered cell treated as if its composition were homogeneous, a reasonable engineering assumption since the cover glass properties were similar to the silicon and the cover represented but 20% of the covered cell thickness. The following relationships were used[15] from elastic beam theory to determine to what extent the cell resists bending
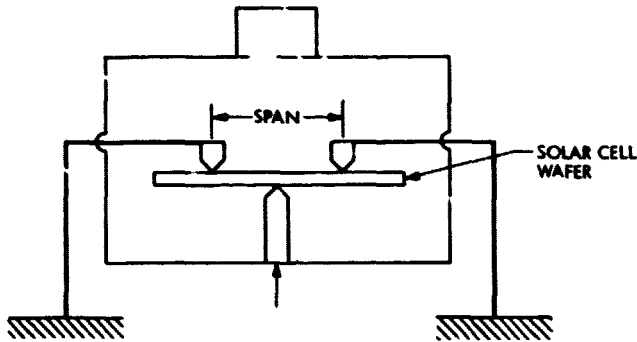
Fig. 26. Schematic of solar cell flexure test fixture

(flexural modulus, E_b), and the stress causing cell failure (flexural failure stress, f_b):

$$E_b = \frac{L^3 (P_2 - P_1)}{4b\, t^3\, (Y_2 - Y_1)}$$

where:

E_b = flexural modulus, N/Cm²

L = span length, cm

b = specimen width, cm

t = thickness, cm

$P_2 - P_1$ = load in Newtons corresponding to the deflection $Y_2 - Y_1$ from a tangent line drawn in relation to the straightest portion on load deflection diagram

$Y_2 - Y_1$ = deflection in cm

and

$$f_b = \frac{3\, PL}{2b\, t^2}$$

where:

f_b = flexural failure stress, N/cm²

P = ultimate load, N

L = span, cm

b = specimen width, cm

t = specimen thickness, cm

Cells were tested in each of four loading modes, 5 cells per mode from each of the three cell categories (bare, ERA, and IPC); 60 cells in total were tested, 20 cells from each category. The test modes for the flexural tests are as they were in Ref. 14:

(1) Mode A: Active surface up, the cell loaded perpendicular to the collector grid fingers.

(2) Mode B: Active surface up, the cell loaded parallel to the collector grid fingers.

(3) Mode C: Active surface down, the cell loaded perpendicular to the collector grid fingers.

(4) Mode D: Active surface down, the cell loaded parallel to the collector grid fingers.

Tables 4 and 5 present the interesting and unexpected test data results. Apparently, the Ferranti cell clad with its integral cover is weaker than the bare cell. One would expect that the integral cover stiffens the cell and makes it more resistant to

Table 4. Average cell flexural modulus[a]

Group	Cell test mode			
	A	B	C	D
Bare	15.55 (22.56)	17.02 (24.68)	18.04 (26.17)	16.18 (23.47)
ERA	13.14 (19.06)	13.35 (19.36)	13.62 (19.75)	13.17 (19.10)
IPC	13.57 (19.68)	13.28 (19.26)	14.20 (20.60)	14.06 (20.39)

[a] In N/cm² x 10⁶ (psi x 10⁶).

Table 5. Average cell flexural stress to failure[a]

Group	Cell test mode			
	A	B	C	D
Bare	23.81 (34.53)	25.35 (36.77)	39.80 (57.72)	34.49 (50.03)
ERA	21.44 (31.10)	21.08 (30.57)	24.51 (35.55)	24.06 (34.90)
IPC	24.72 (35.85)	19.14 (27.76)	27.64 (40.09)	26.32 (38.17)

[a] In N/cm² x 10³ (psi x 10³).

fracture. The test data indicate it does neither; instead, the integrally covered cells bend and fracture more easily than do the bare cells.

The data indicate a slight increase in the strength of IPC covered cells above bare cells, 3.8% in Mode A in Table 5, but in all other test modes the IPC and ERA covered cells show diminished strength. ERA covered cells in Mode C declined in strength more than 38%. The bare and covered are strongest when loaded upon their reverse surface, particularly in the direction perpendicular to the grid lines (Mode C). However, it is also in this mode that the covered cell lost strength to the greatest extent, averaging a 34.5% decline. The average strength loss for IPC covered cells was 18.8%, and for ERA covered cells, 23.8%. No data at hand relates individual aspects of the sputtering processes to this evidence of cell strength loss. Special test parameters used in this test and the test data are presented in the Appendix.

4. Change in cell electrical performance characteristics resulting from integral cover application. These changes are the result of cell preparation for the sputtered cover, the sputtering process, the sputtered glass film, and the MgF_2 AR coating upon the integral cover. According to ERA and IPC cell data, the performance of most cells declined after processing.

Of the 71 ERA integrally covered cells that met mechanical and electrical specifications, the average short circuit current declined 3.17 mA, or 2.34%, the standard deviation being 1.94 mA if this sample truly represented a large production lot.

Of the 77 IPC covered cells that met mechanical and electrical specif s after the integral cover process, the average current ed when the cell was tested at 0.485 V declined 4.79 mA, or 3.54%, with the estimated standard deviation at 2.08 mA. IPC made no short circuit current measurements.

Lacking a test fixture to mechanically mount wraparound solar cells for electrical test, the IPC newly designed test gear for these tests did not attain desired measurement repeatability. This could account for the greater electrical performance data dispersion than obtained from ERA processed cells.

5. Electrical characterization of the integrally covered cell. This test was multipurpose, with one purpose of the study being to characterize the electrical performance of the bare and integrally covered cells. How well the integral cover depositions withstood the test conditions formed the other part of the study.

Five cells from each of the categories were mounted on a specially designed test plate. The cells were selected from those grouped about the median in their electrical performance test in simulated AMO at 135.3 mW/cm^2, 28°C. They were also free of mechanical defects.

Kovar ribbon was used as cell interconnects to obtain a close thermal expansion coefficient match to silicon because of the wide test temperature range. Normally, the ribbon is attached to the cell and then manually formed to the requirements of the circuit. However, some of the Ferranti cells broke if an attached interconnect was reshaped during the assembly of a prototype test plate. Instead, the interconnects for these cells were first preformed with stress relieved loops before attachment to cells, and interconnect redressing in the final assembly was kept to a minimum after attachment to cell.

The cells were then bonded to the 3.18-mm (0.125-inch) thick copper test plate with GE RTV 560/T12 silicone adhesive. The adhesive layer serve as dielectric between cells and plate. Electrical connection of the cells to printed circuitry on the plate completed a four-wire circuit system to each cell that isolated the voltage sensing leads from those carrying current. The voltage drop in the current carrying leads would otherwise affect the voltage data.

A copper-constantan thermocouple attached to a bare cell with Ecobond 57C silver conductive cement monitored cell temperature, and a proportional temperature controller maintained cell temperature within ±0.5°C as data was recorded. An earlier study at JPL that used six thermocouples mounted on a similar test plate demonstrated that the temperature of the 15 cells were virtually identical at equilibrium within the resolution of the test equipment. This eliminated the need for plate modification to adjust thermal gradients.

The test plate was mounted vertically behind a quartz window of a thermal vacuum test chamber that was evacuated to 30 microns. The chamber was first purged with dry nitrogen to avoid dew point condensates during the temperature excursions. Cells on the plates were illuminated through the quartz window with a Spectrolab Model X25 Mark II solar simulator. Balloon flight standard cells[16] provided intensity and light flux spectral quality references. A tabulation of the matrix of light intensity and cell temperature variations used in this study is presented in Table 6. Electrical performance data was recorded for each cell on the test plate at each condition in Table 6, and this data was averaged for the cells within each of the three categories. This solar cell electrical performance characteristics test is similar to others performed at JPL.[17, 18]

	Light intensity, mW/cm²					
	241.6	135.3	96.6	48.3	24.2	4.8
	-60	-80	-100	-120	-160	-160
	-40	-60	-80	-100	-140	-140
	-20	-40	-60	-80	-120	-120
	0	-20	-40	-60	-100	-100
	20	0	-20	-40	-80	-60
Cell	40	20	0	-20	-60	-60
temperature	60	40	20	0	-40	-40
°C	80	60	40	20	-20	-20
	100	80	60	40	0	0
	120	100	80	60	20	20
	140	120	100	80	40	4
		140	120	100	60	
			140	120		
				140		

I_{sc}, V_{oc}, P_{max}, and curve factor (CF) averages for the three cell groups are presented in Fig. 27. The electrical performance differences among the three groups are subtle in these plots, and the differences are better revealed with bare cell data averages subtracted from those of ERA and IPC integrally covered cells. Percent differences of the electrical parameters between bare cell and each integral cover process are shown in Figs. 28 and 29. Figure 28 displays percent changes of I_{sc} and V_{oc} in the Ferranti cell after integral cover depositions, and Fig. 29 displays the percent changes in P_{max} and CF.

The electrical performance of ERA covered cells is seen to benefit more from the integral cover application than do the IPC covered cells. V_{oc} and P_{max} of the ERA processed cells particularly display gains over the bare cell, in excess of 10% in some test conditions. However, because of evidence of integral cover delamination similar to that found earlier (see Subparagraph III-A-3-b), the apparent electrical performance gains of the ERA covered cells are misleading.

6. Cover delamination resulting from temperature extremes. The reason for the electrical performance gain is shown in photos of the test plate in Fig. 30. ERA covered cells are in the center column. IPC covered cells are in the column left of center, and the bare cells are in the column on the right.

The integral covers delaminated as they did after the thermal cycling tests, as shown in Fig. 15. ERA processed covers again delaminated to a greater extent than IPC processed covers, and again at the upper and lower surfaces of the MgF_2 coating. As before, the IPC covers delaminated only at the upper MgF_2 surface (see Subparagraph III-A-3-b). The relative severity of delamination explains the data of Figs. 28 and 29. The Ferranti cells operated cooler under the ERA

integral covers because of more extensive cover delamination. Cells under the IPC covers were warmer because of the relatively lower thermal resistance between the cells and their covers, which delaminated to a lesser extent. Consequently, the more temperature sensitive the electrical parameter, the better the performance of the ERA covered cell appeared. Heat from the solar simulator light flux transferred most readily to the bare cells and more readily to the cells under the IPC processed covers than to those under the ERA covers.

IV. Conclusions

Lightweight components are indispensable in the pursuit of solar arrays with more desirable specific power characteristics, but the lightweight components examined in this study displayed noteworthy disadvantages as well. Their weaknesses may be eliminated or reduced with future process or application refinement, and for our conclusions we list these weaknesses as revealed in this study. Advantages of the components and rationale for their initial selection were discussed in Section II.

A. Solar Cell

Production economy becomes a major consideration for a product requiring many expensive and complex manufacturing processes, particularly if the product is as fragile as the solar cell, and vulnerable to fatal damage. Functional reliability becomes a major consideration when so fragile a product as a solar cell contributes to the electrical power requirements of a spacecraft. Halving cell thickness appears to about double handling losses. About 5% breakage losses is reported for solar cells 305 to 381 microns (12 to 15 mils) thick, 10% for 203 microns (8 mils) thick, and 20% losses for cells 127 microns (5 mils) thick.[10] Breakage with the 127-micron Ferranti cell was also unusually high at JPL during this study. Cells this thin may signal a crossover in device reliability, not only for the cells' ability to survive with acceptable yield the processes leading to final solar array asembly, but also for their ability to withstand spacecraft launch stresses, thermal stress, array deployment, and the multiple array retraction and redeployment sequences in space flight that have been proposed for some missions.

B. Sputtered Integral Cover

The sputtered integral cover is still in the development stage. With further work and time, the following difficulties are concerns may be eliminated: The sputtering process requires flaw-free solar cells (see Subparagraph III-B-1) that are expensive. Glass is presently sought with characteristics that are more oriented to needs of the sputtering process and the mechanical limits of the cell than to the optical requirements of a solar cell cover (see Subparagraph II-B-2-a).

BARE FERRANTI CELLS
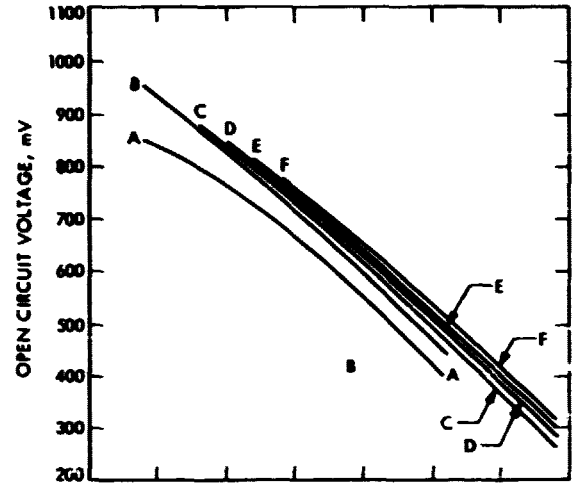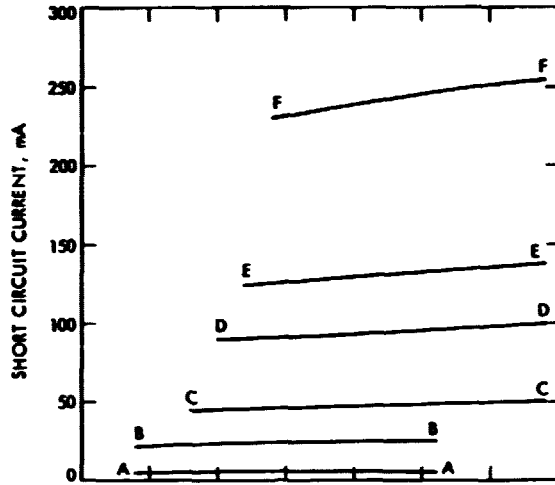
FERRANTI CELLS WITH INTEGRAL COVERS PROCESSED BY ELECTRICAL RESEARCH ASSOCIATION
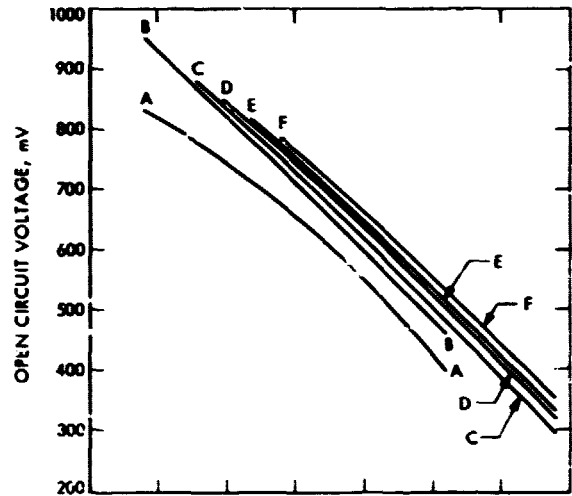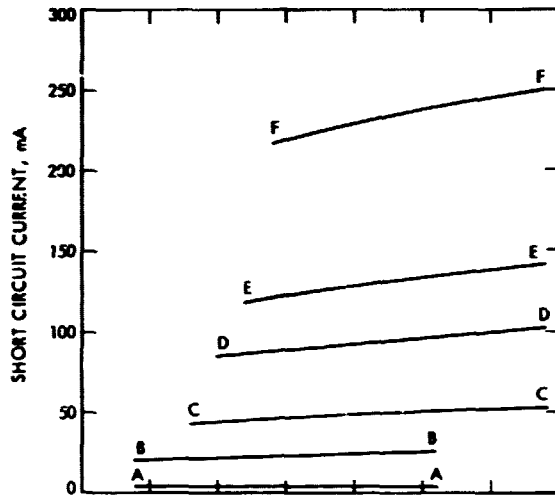
FERRANTI CELLS WITH INTEGRAL COVERS PROCESSED BY ION PHYSICS CORPORATION
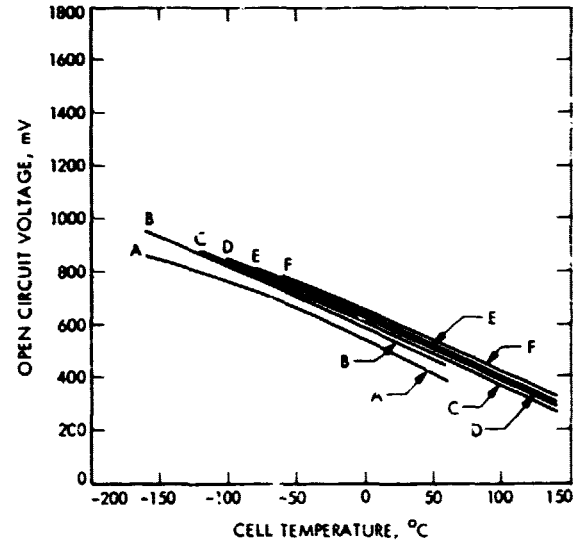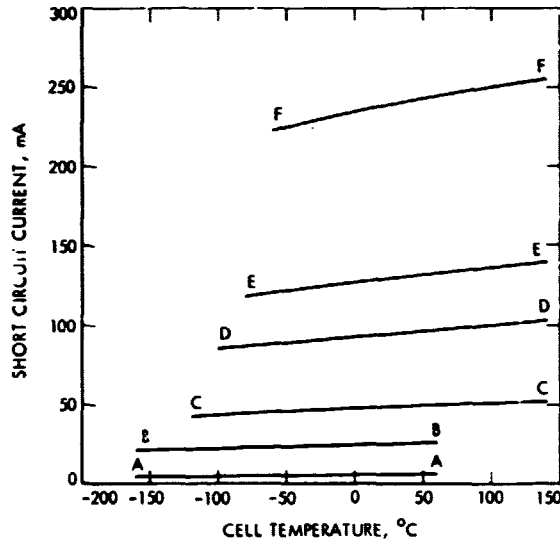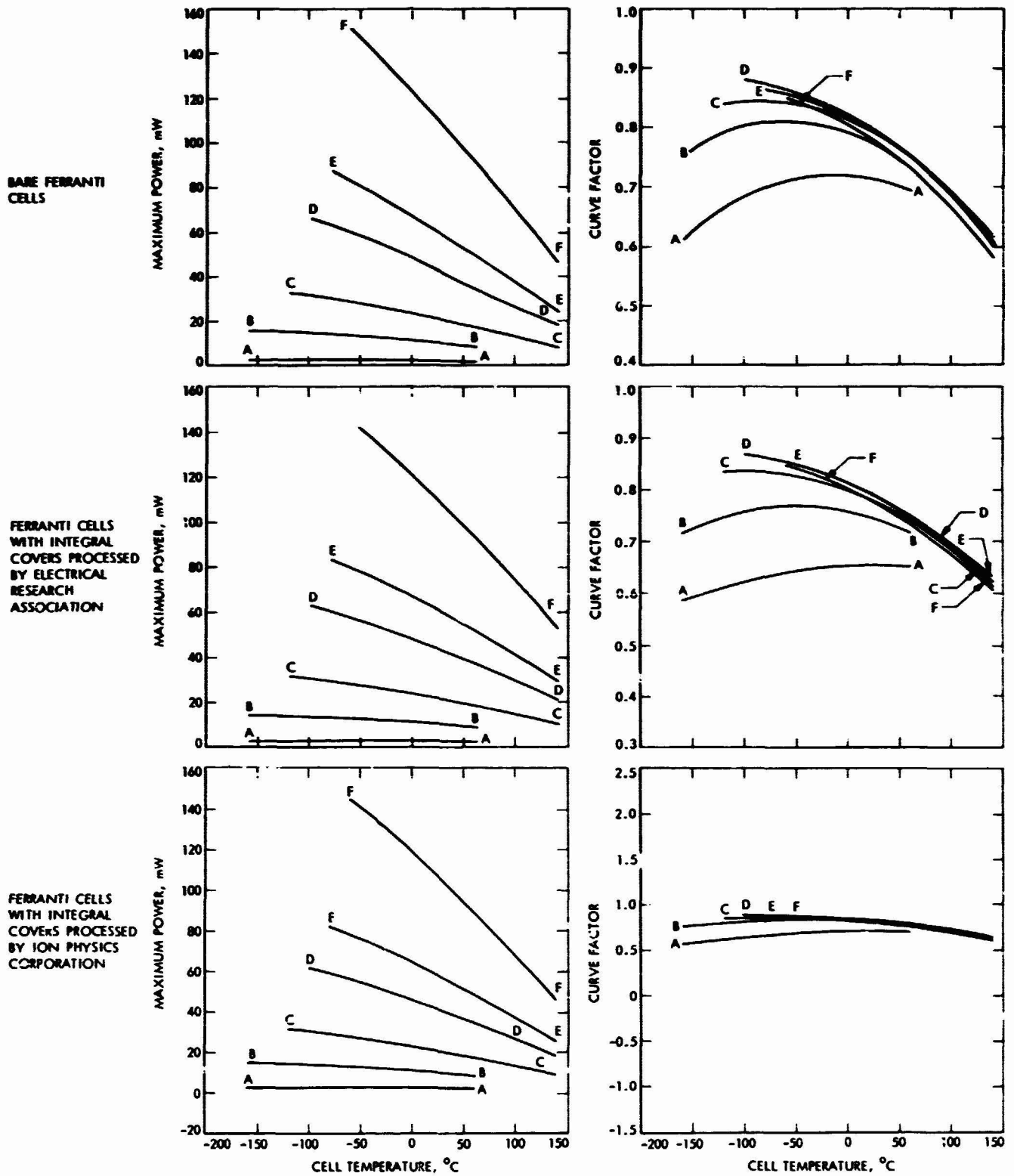
Fig. 27. Comprehensive electrical performance characteristics of bare and integrally covered Ferranti cells. Simulated solar intensities are given in mW/cm² where A = 4.8, B = 24.2, C = 48.3, D = 96.6, E = 135.3, and F = 241.6
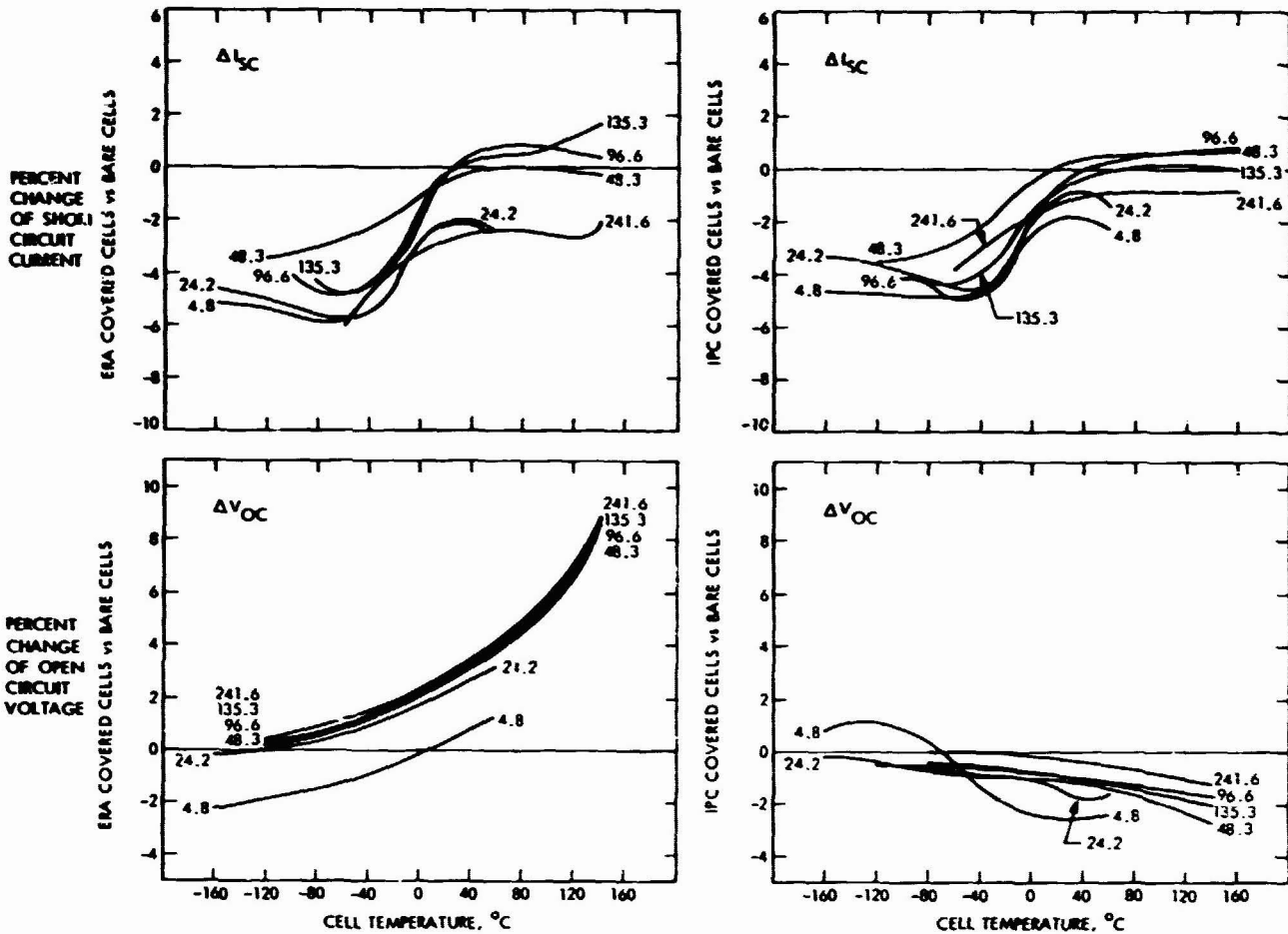
Fig. 28. Percent changes in I_{sc} and V_{oc} in integrally covered Ferranti cells. Simulated solar intensities are in mW/cm²

The ion flux in the RF sputtering process is a hazardous environment for a solar cell (see Subparagraph III-B-2-h) that will require careful management to avoid solar cell damage. The electron flux also present can darken the deposited sputtered cover glass (see Subparagraph III-B-2-i).

So dependent is a spacecraft upon its electrical power source, that a solar array designer hesitates to place so brittle and fragile a material as a solar cell under any additional stress. Although DC 7070 exhibits the least intrinsic stress in sputtered form of any glass yet tested, it nonetheless imparts a magnitude of stress to the cell that is about equal to, and in addition to, the thermal stress the cover imparts at typical operating temperatures (see Subparagraph III-B-2-a).

The sputtered cover, with its processes, weakens the integrally covered cell to the extent that an uncovered cell appears stronger (see Subparagraph III-B-3-d). Sputtering chamber debris (see Subparagraph II-B-2-g) and carrot defects (Subparagraph III-B-2-j) may act in space operations as solar concentrators that could damage the covered cell system. Inherent in the solar cell are edges that impart stress areas to the sputtered glass cover that could affect its reliability (see Subparagraph III-B-1).

This study reveals a major weakness in sputtered integral cover adhesion to the MgF$_2$ AR coating on the cell (Subparagraphs III-A-3-b and III-B-6) that raises concern regarding the reliability of sputtered covers upon solar cells in storage and after exposure to space environmental conditions, particularly of the design examined. Sputtered integral covers lack optical flatness. When the array is misoriented to the sun during space operations, this lack of flatness could result in greater array power output loss than it would experience with discrete covers.

C. Array Model Substrate

Solar cell delaminations from the model flexible substrate after thermal cycling tests suggest the need for thermal stress-relieved interconnections for the wraparound cell.

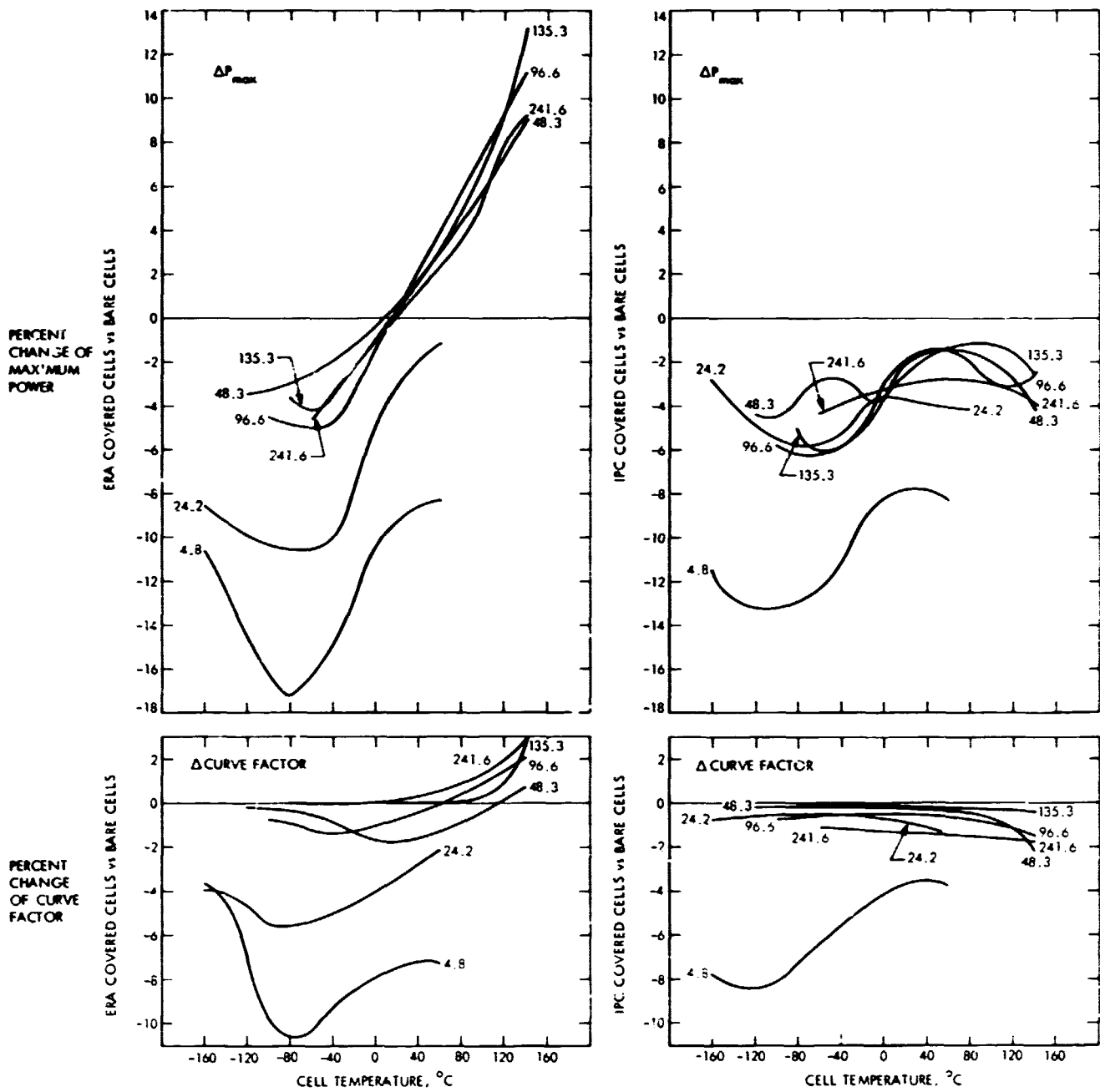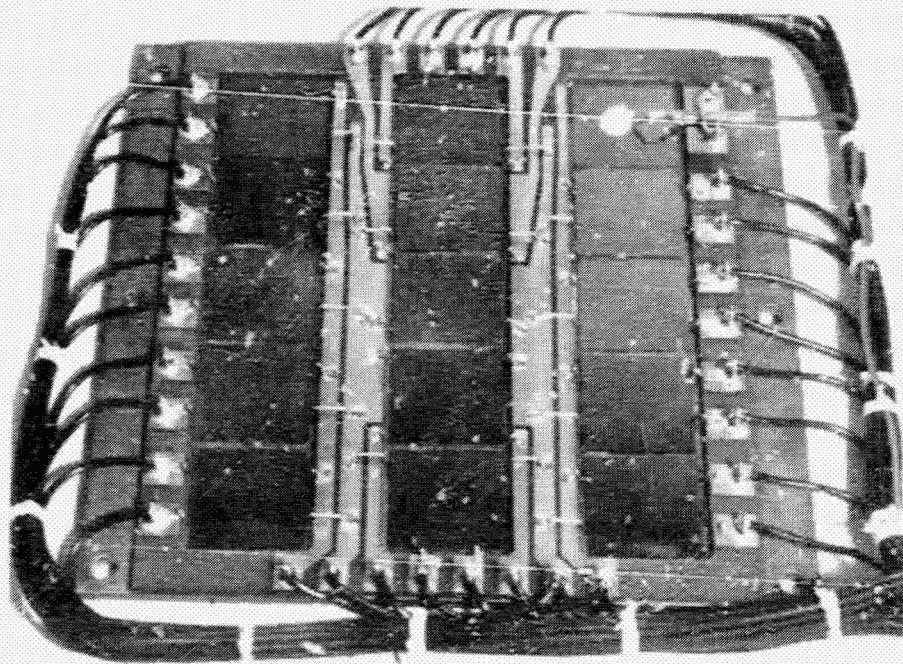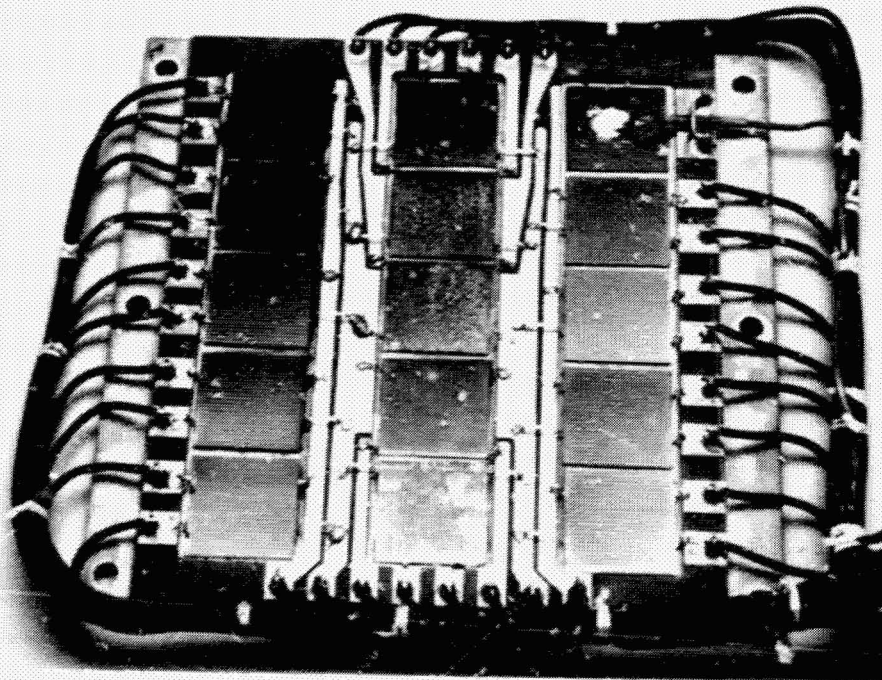Fig. 29. Percent changes in P_{max} and CF in integrally covered Ferranti cells. Simulated solar intensities are in mW/cm²

(a) BEFORE TEST START

(b) AFTER TEST COMPLETION

Fig. 30. Cell test plate for the combined environmental test: cells in
the center column have integral covers processed by ERA; cells in
the column left of center have integral covers processed by IPC;
cells in the remaining column are uncovered.

References

1. Brackley, G., et al., *Development of Integral Covers for Silicon Solar Cells*, ESRO CR-215. Electrical Research Association, Surrey, England, November 1974.

2. Brackley, G., et al., *Develop.nent of Integral Covers for Silicon Solar Cells*, ESRO CR-44. Electrical Research Association, Surrey, England, July 1971.

3. Brackley, G., et al., *Development of Integral Covers for Silicon Solar Cells*, ESRO CR-68. Electrical Research Association, Surrey, England, November 1972.

4. Brackley, G., et al., "Integral Covers for Silicon Solar Cells," in *Proceedings of the 9th Photovoltaic Specialists Conference*, Silver Spring, Md., May 3-4, 1972, pp. 174-178. IEEE, New York, 1972.

5. Brackley, G., et al., *Development of Integral Covers for Silicon Solar Cells*, ESRO CR-16. Electrical Research Association, Surrey, England, May 1970.

6. Brenner, A. B., and Senderoff, S., J. Res. Nat. Bur. Stand., *42*, pp. 105-123, 1949.

7. Hill, G. J., and Lawson, K., *Final Report on JPL Contract AQ-621759*. Electrical Research Association, Surrey, England.

8. Gardner, J. A., *Solar Electric Propulsion System Integration Technology Final Report*. Technical Memorandum 33-583, Vol. 2. Jet Propulsion Laboratory, Pasadena, California, November 15, 1972.

9. Treble, F. C., "Status Report on Royal Aircraft Establishment Advanced Solar Array Development," in *Proceedings of the 9th IEEE Photovoltaic Specialist Conference*, Silver Spring, Md., May 3-4, 1972. IEEE, New York, 1972.

10. Berman, R., *Thin Cell Integral Coverslips*, Final Report on JPL Contract No. AQ 621760. Ion Physics Corporation, Burlington, Mass., April, 1975.

11. Vossen, J. L., and O'Neill, J. J., *RF Sputtering Processes*, RCA Review. Radio Corporation of America Laboratory, Princeton, New Jersey, June 1968.

12. Brackley, G., et al., *Development of Integral Covers for Silicon Solar Cells*, ESRO CR-32. Electrical Research Association, Surrey, England, September 1970.

13. Cistola, A. B., in *Solid State Technology*, Vol. 15, No. 12, pp. 36-40, 1972.

14. Salama, A. M., et al., *Stress Analysis and Design of Silicon Solar Arrays and Related Material Properties*, Technical Report 32-1552. Jet Propulsion Laboratory, Pasadena, California, March 1972.

15. *Standard Method of Test for Flexural Properties*, Part 35, p. 288. American Society for Testing Materials.

16. Greenwood, R. F., and Mueller, R. L., *Results of the 1970 Balloon Flight Solar Cell Standardization Program*. Technical Report 32-1575. Jet Propulsion Laboratory, Pasadena, California, December 1, 1972.

17. Patterson, R. E., and Yasui, R. K., *Parametric Performance Characteristics and Treatment of Temperature Coefficients of Silicon Solar Cells for Space Application*. Technical Report 32-1582. Jet Propulsion Laboratory, Pasadena, California, May 1973.

18. Berman, P., *Preliminary Investigation of Integral Coverglasses Applied to Ferranti Cells*, Engineering Memorandum 342-329. Jet Propulsion Laboratory, Pasadena, California, March 1976. (JPL internal document.)

Appendix
Data Results of Three-Point Flexure Tests

Flexure test parameters: wafer span = 1.27 cm (0.5 in.)

Instron crosshead speed = 0.051 cm
(0.02 in.)/min

chart speed = 12.7 cm (5 in.)/min

Table A-1. Ware Ferranti cells

Cell ID and test mode[a]	Ultimate load, N (lb)	Cell width, cm (in.)	Average cell thickness t, 10^{-2} cm (10^{-3} in.)	Flexural stress to failure, 10^3 N/cm^2 (10^3 psi)	Flexural modulus, 10^6 N/cm^2 (10^6 psi)
Mode A					
28	4.893 (1.10)	2.006 (0.7897)	1.468 (5.78)	21.57 (31.28)	15.66 (22.71)
36	6.094 (1.37)	2.003 (0.7887)	1.483 (5.84)	26.34 (38.20)	15.54 (22.54)
44	5.427 (1.22)	2.005 (0.7892)	1.494 (5.88)	23.82 (33.54)	15.22 (22.07)
52	5.604 (1.26)	2.004 (0.7891)	1.521 (5.99)	23.02 (33.38)	15.72 (22.80)
60	6.049 (1.36)	2.005 (0.7893)	1.516 (5.97)	25.00 (36.26)	15.65 (22.70)
Mode B					
30	6.894 (1.55)	2.004 (0.7889)	1.468 (5.78)	30.47 (44.19)	14.67 (21.28)
38	5.070 (1.14)	2.002 (0.7883)	1.435 (5.65)	23.43 (33.98)	15.34 (22.25)
46	6.272 (1.41)	2.004 (0.7891)	1.582 (6.23)	23.78 (34.49)	15.50 (22.48)
54	6.049 (1.36)	2.004 (0.7891)	1.486 (5.85)	26.04 (37.77)	15.00 (21.75)
62	4.359 (0.98)	2.004 (0.7891)	1.341 (5.28)	23.04 (33.41)	24.57 (35.64)
Mode C					
32	11.965 (2.69)	2.004 (0.7889)	1.600 (6.30)	44.42 (64.43)	16.38 (23.76)
40	12.810 (2.88)	2.005 (0.7894)	1.572 (6.19)	49.18 (71.33)	16.40 (23.78)
48	10.319 (2.32)	2.004 (0.7889)	1.412 (5.56)	49.13 (71.26)	22.99 (33.35)
56	6.894 (1.55)	2.004 (0.7891)	1.412 (5.56)	32.81 (47.59)	17.04 (24.72)
64	5.649 (1.27)	2.005 (0.7892)	1.514 (5.96)	23.43 (33.98)	17.40 (25.24)
Mode D					
34	5.960 (1.34)	2.001 (0.7877)	1.552 (6.11)	23.57 (34.18)	15.89 (23.04)
42	8.540 (1.92)	2.009 (0.7908)	1.409 (5.54)	40.81 (59.19)	16.02 (23.24)
50	10.987 (2.47)	2.004 (0.7891)	1.463 (5.76)	48.78 (70.75)	16.61 (24.09)
58[b]					
66	6.272 (1.41)	2.004 (0.7690)	1.549 (6.10)	24.81 (35.98)	16.21 (23.51)

[a]See Subparagraph III-B-3-d.

[b]Cell broken prior to test.

PRECEDING PAGE BLANK NOT FILMED

Table A-2. ERA covered Ferranti cells

Cell ID and test mode[a]	Ultimate load, N (lb)	Cell width, cm (in.)	Average cell thickness t, 10^{-2} cm (10^{-3} in.)	Flexural stress to failure, 10^3 N/cm^2 (10^3 psi)	Flexural modulus, 10^6 N/cm^2 (10^6 psi)
Mode A					
28	7.740 (1.74)	2.015 (0.7932)	1.702 (6.70)	25.27 (36.65)	13.43 (19.48)
36	7.450 (1.675)	2.008 (0.7907)	1.600 (6.30)	27.60 (40.03)	13.28 (19.26)
44	3.759 (0.845)	2.011 (0.7919)	1.781 (7.01)	11.23 (16.28)	12.44 (18.04)
52	7.028 (1.58)	2.011 (0.7918)	1.737 (6.84)	22.05 (31.98)	13.39 (19.42)
60	6.894 (1.55)	2.011 (0.7916)	1.760 (6.93)	21.08 (30.58)	13.18 (19.12)
Mode B					
30	6.316 (1.42)	2.010 (0.7915)	1.636 (6.44)	22.37 (32.45)	12.74 (18.47)
38	3.247 (0.73)	2.001 (0.7877)	1.641 (6.46)	11.49 (16.66)	12.87 (18.67)
46	7.740 (1.74)	2.007 (0.7901)	1.702 (6.70)	25.37 (36.79)	14.84 (21.53)
54	7.295 (1.64)	2.000 (0.7873)	1.648 (6.49)	25.57 (37.09)	13.51 (19.60)
62	6.761 (1.52)	2.008 (0.7906)	1.765 (6.95)	20.58 (29.85)	12.78 (18.54)
Mode C					
32	7.762 (1.745)	2.010 (0.7913)	1.808 (7.12)	22.50 (32.63)	12.82 (18.60)
40	6.028 (1.535)	2.010 (0.7913)	1.600 (6.30)	25.28 (36.66)	13.61 (19.74)
48	7.762 (1.745)	2.011 (0.7917)	1.730 (6.81)	24.57 (35.64)	14.00 (20.30)
56	7.117 (1.60)	2.009 (0.7910)	1.621 (6.38)	25.70 (37.27)	14.02 (20.34)
Mode D					
34	7.962 (1.79)	2.006 (0.7896)	1.745 (6.87)	28.45 (41.26)	12.84 (18.61)
42	8.540 (1.92)	2.001 (0.7676)	1.701 (6.73)	27.84 (40.37)	13.23 (19.19)
56	5.338 (1.20)	2.005 (0.7895)	1.704 (6.71)	17.46 (25.32)	13.32 (19.32)
58	7.206 (1.62)	2.008 (0.7906)	1.742 (6.86)	22.51 (32.65)	13.29 (19.28)

[a] See Subparagraph III-B-3-d.

Table A-3. IPC covered Ferranti cells

Cell ID and test mode[a]	Ultimate load, N (lb)	Cell width, cm (in.)	Average cell thickness t, 10^{-2} cm (10^{-3} in.)	Flexural stress to failure, 10^3 N/cm^2 (10^3 psi)	Flexural modulus, 10^6 N/cm^2 (10^6 psi)
Mode A					
42	8.318 (1.87)	2.009 (0.7910)	1.707 (6.72)	27.07 (39.26)	13.58 (19.69)
50	4.848 (1.09)	2.009 (0.7910)	1.656 (6.52)	20.21 (29.31)	14.25 (20.66)
58	6.138 (1.38)	2.006 (0.7896)	1.643 (6.47)	21.59 (31.31)	14.36 (20.82)
66	7.562 (1.70)	2.007 (0.7901)	1.562 (6.15)	29.41 (42.66)	13.18 (19.12)
70	7.339 (1.65)	2.008 (0.7904)	1.659 (6.53)	25.32 (36.72)	13.46 (19.52)
Mode B					
44	6.094 (1.37)	1.999 (0.7870)	1.687 (6.64)	20.42 (29.61)	12.74 (18.48)
52	5.115 (1.15)	2.005 (0.7895)	1.527 (6.01)	20.85 (30.24)	13.98 (20.28)
60	4.537 (1.02)	2.007 (0.7902)	1.557 (6.13)	17.76 (25.76)	14.05 (20.38)
67	5.871 (1.32)	2.012 (0.7922)	1.692 (6.66)	19.42 (28.17)	12.89 (18.69)
71	4.848 (1.09)	2.011 (0.7919)	1.631 (6.42)	17.27 (25.04)	12.72 (18.45)
Mode C					
46	7.428 (1.67)	2.007 (0.7902)	1.638 (6.45)	25.95 (37.64)	14.35 (20.81)
54	9.385 (2.11)	2.005 (0.7894)	1.588 (6.25)	35.39 (51.32)	15.09 (21.89)
62	6.850 (1.54)	2.007 (0.7903)	1.575 (6.20)	26.21 (38.02)	14.01 (20.32)
68	9.118 (2.05)	2.007 (0.7903)	1.732 (6.82)	28.84 (41.83)	13.96 (20.25)
72	6.583 (1.48)	2.007 (0.7903)	1.692 (6.66)	21.83 (31.66)	13.61 (19.74)
Mode D					
48	7.695 (1.73)	2.006 (0.7897)	1.605 (6.32)	28.36 (41.13)	15.67 (22.73)
56	7.740 (1.74)	2.010 (0.7912)	1.593 (6.27)	28.93 (41.96)	14.09 (20.43)
64	11.076 (2.49)	2.009 (0.7911)	1.697 (6.68)	36.47 (52.90)	13.94 (20.21)
69	5.249 (1.18)	2.011 (0.7917)	1.679 (6.61)	17.64 (25.58)	13.19 (19.13)
73	5.427 (1.22)	2.000 (0.7874)	1.600 (6.30)	20.19 (29.28)	13.40 (19.44)

[a]See Subparagraph III-B-3-d.

Table A-4. Mean standard deviation calculations for the cell flexure parameters

	Width, mm (in.)	Thickness micron (mil)	Flexural stress, 10^3 N/cm^2 (10^3 psi)	Flexural modulus, 10^6 N/cm^2 (10^6 psi)
Bare	$20.043 \pm 1.50 \times 10^{-2}$	148.84 ± 6.68	30.68 ± 0.708	12.61 ± 1.021
	($0.7891 \pm 5.90 \times 10^{-4}$)	($5.86 \pm 2.7 \times 10^{-1}$)	(44.49 ± 1.027)	(18.290 ± 1.481)
ERA	$20.079 \pm 4.11 \times 10^{-2}$	170.18 ± 6.35	22.61 ± 0.495	13.31 ± 0.057
	($0.7905 \pm 1.62 \times 10^{-3}$)	($6.70 \pm 2.5 \times 10^{-1}$)	($32.79 \pm 7.182 \times 10^{-1}$)	($19.306 \pm 8.2776 \times 10^{-2}$)
IPC	$20.079 \pm 3.30 \times 10^{-2}$	163.58 ± 5.59	24.28 ± 0.585	13.82 ± 0.074
	($0.7902 \pm 1.30 \times 10^{-3}$)	($6.44 \pm 2.2 \times 10^{-1}$)	($35.22 \pm 8.453 \times 10^{-1}$)	($20.052 \pm 1.076 \times 10^{-1}$)